The College of William and Mary

PIONIC X-RAY YIELDS AND LEVEL BROADENING IN LOW-Z ATOMS

by

William Wade Sapp, Jr.

August, 1970

WM 70-21

PHYSICS DEPARTMENT

Williamsburg, Virginia

Supported in part by

NATIONAL AERONAUTICS AND SPACE ADMINISTRATION

PIONIC X-RAY YIELDS AND LEVEL BROADENING IN LOW-Z ATOMS

by

William Wade Sapp, Jr.

August, 1970

WM 70-21

Supported in part by the

National Aeronautics and Space Administration

Contract NASA NGL 47-006-008

The report is based in part on a dissertation submitted by the author to the Department of Physics, College of William and Mary, in partial fulfillment of the requirements for the degree of Doctor of Philosophy.

PIONIC X-RAY YIELDS AND LEVEL BROADENING IN LOW-Z ATOMS

TABLE OF CONTENTS

ABSTRACT

Absolute intensities of pionic and muonic x-ray transitions in Li^6, Be^9, C, O, Mg, and Ti have been measured in thin, elemental targets (except for H_2O) using Si(Li) and Ge(Li) spectrometers. The pionic K-transitions in targets with $Z \leq 8$ and L-transitions in all targets except Li^6 are examined in order to study the absorption process of negative pions in complex nuclei.

A pionic-cascade calculation which was constrained to reproduce the observed yields predicted population probabilities for the lower levels of the mesic atoms and gave values for the strong-interaction level widths. It was also used to predict a nuclear capture schedule for π^- in Li^6. The 2p-level broadenings are 0.015 ± 0.005 eV for Li^6, 0.16 ± 0.03 eV for Be^9, 2.6 ± 0.9 eV for C^{12}, and 12 ± 4 eV for O^{16}. The latter two results are a factor of 2.5 larger than the values obtained in a recent experiment which employed somewhat different techniques. The present results are in satisfactory agreement with predictions based on a phenomenological optical potential whose constant parameters had been determined from selected pionic x-ray data. The parameters for the imaginary part of this potential are larger by a factor of two than those predicted by the quasi-deuteron absorption model.

I. INTRODUCTION

Transitions in mesic atoms and the interaction of the bound-state meson with the nucleus have been the object of considerable attention over the past two decades.[1] Low energy negative mesons coming to rest in a target typically become bound to a target atom in the final step of the slowing-down process. Transitions which occur in the cascade toward the atomic ground state result in the emission of Auger electrons and x rays. The energy, line width, and intensity of the characteristic x rays have been measured to obtain information on nuclear radii, nuclear moments, the meson mass, and pion-nucleus interaction parameters. In particular the intensity or yield of a given pionic transition, defined as the number of emitted x rays per stopped meson, can be used to explore the cascade scheme and the absorptive part of the pion-nucleus interaction.

The discovery of the "missing x ray" anomaly[2] suggested that the yields in low-Z elements could not be predicted from known atomic cascade processes. Several experimental[5-8] and theoretical[9-14] studies, stimulated in part by this discovery, have been directed toward understanding the processes which influence the cascade in mesic atoms. These studies are of interest despite recent corrections[15,16] of the earlier experimental data.

If the atomic processes are sufficiently well understood to allow an accurate prediction of the population probability $P_{n\ell}$ of the

atomic level characterized by (n,ℓ), then the pionic x-ray yield $Y_{n\ell}^{n'\ell'}$ (radiative) for the mesic transition $(n,\ell)\rightarrow(n',\ell')$ provides a direct measure of the nuclear capture rate $\Gamma_{n\ell}(\text{cap})$ from the initial state. If the yield is written in the form

$$Y_{n\ell}^{n'\ell'}(\text{rad}) = \frac{P_{n\ell}\,\Gamma_{n\ell}^{n'\ell'}(\text{rad})}{\Gamma_{n\ell}(\text{cap}) + \Gamma_{n\ell}(\text{e.m.})} \quad , \tag{1a}$$

then

$$\Gamma_{n\ell}(\text{cap}) = \frac{P_{n\ell}\,\Gamma_{n\ell}^{n'\ell'}(\text{rad})}{Y_{n\ell}^{n'\ell'}(\text{rad})} - \Gamma_{n\ell}(\text{e.m.}) \quad , \tag{1b}$$

where

$$\Gamma_{n\ell}(\text{e.m.}) = \sum_{n''\ell''} \Gamma_{n\ell}^{n''\ell''}(\text{radiative}) + \sum_{n''\ell''} \Gamma_{n\ell}^{n''\ell''}(\text{Auger})$$

is the total electromagnetic decay rate, the summation being over all allowed final states. Only electric-dipole transitions are considered in the calculation of $\Gamma_{n\ell}(\text{e.m.})$ since the rates for the higher-order multipoles are insignificant in comparison. These E1 rates are generally calculated using hydrogenic wave functions for the pionic bound states. However, for K-series transitions the relatively large strong-interaction distortion of the 1s-state wave function makes necessary a more exact treatment even for low-Z elements. The non-radiative processes of collisional (external) Auger transitions, Stark mixing, and meson decay are ignored because their contributions to the total decay rate are negligible for the mesic levels of interest.[10]

The yield $Y_{n\ell}^{n'\ell'}(\text{rad})$ is measured experimentally and $P_{n\ell}$ deduced from either atomic-cascade calculations, or observations of other

x-ray transitions, or both. The nuclear capture rate or, equivalently, the level width can in this way be determined for levels whose broadening is too small to be measured directly,[17] and the range over which theoretical predictions may be tested can thus be extended.

Recent experiments[19,20] as interpreted by Krell and Ericson[21] indicated that either their theoretical model does not satisfactorily describe the 2p-state widths for all elements or a systematic uncertainty exists in one or both of the experimental methods used to determine these widths.

Because the most dramatic discrepancies existed for elements with $Z \leq 11$, it was the primary purpose of the present investigation to determine the 2p-state widths of selected elements in this region with an experimental technique different from that of Refs. 19, 20. The 2p-level widths for Li^6 and Be^9 reported here are consistent with recently reported values[16,20] from other laboratories, while the previously published[20] 2p-level widths in C and O are substantially smaller than those obtained in the present investigation. The results of the present work compare favorably to predictions based on an optical potential whose constant parameters have been previously determined from selected pionic x-ray data. However, the values of the parameters for the absorptive part of the potential are in disagreement with the predictions of Krell and Ericson which are based on the quasi-deuteron model. A secondary purpose of this investigation was to determine the capture schedule for π^- in Li^6 for which no previous measurements exist. The capture schedules are of particular interest to those engaged in the theoretical study of pion capture in complex nuclei.[22]

The measurements made here and their interpretation will be described as follows: In Sec. II, theories pertaining to nuclear absorption of low energy pions are reviewed; Sec. III describes the experimental technique and the general data accumulation procedure; in Sec. IV, analysis of the x-ray spectra is described, the detector-efficiency measurements are discussed, and the absolute yields are determined; Sec. V describes the calculation of the cascade scheme and the determination of the absorption rates; and in Sec. VI the experimental results are summarized and compared to earlier work and to theoretical predictions.

II. THEORY

Pion absorption in the nucleus is known to be a short-range phenomenon occurring predominantly on nucleon pairs. The short-range nature of the interaction enabled West[9] to describe the n, ℓ, and Z dependence of the nuclear absorption rate in terms of the overlap of the square of the pion wave function with the nuclear volume. A short-range interaction was also implicit in the π-mesic x-ray yield analysis of Eisenberg and Kessler,[13] who characterized the interaction with a single variable, the lifetime of pions in nuclear matter.

That the absorption should occur on nucleon pairs may be understood from kinematical arguments. Consider first the possibility of absorption by a single free nucleon of mass M initially at rest, $\pi + N \rightarrow N$. If μ is the meson rest mass and P_π its initial momentum, then energy conservation gives

$$\sqrt{P_\pi^2 + \mu^2} + M = \sqrt{P^2 + M^2}$$

where P is the final momentum of the absorbing nucleon, and we have set $c = 1$. Letting $P_\pi = 0$, a good approximation for mesic atoms, we obtain $P \approx \sqrt{2M\mu} = 525$ MeV/c. But momentum conservation requires $\vec{P} = -\vec{P}_\pi = 0$, hence the process is forbidden. However, if the nucleon is initially bound in a nucleus, the residual nucleus is able to compensate for the momentum imbalance, and a single nucleon may be emitted with approximately the above momentum. The nucleon bound-state wave function has Fourier components of relatively small amplitudes with this high momentum (Fermi

momentum is typically 250 MeV/c), thus the wave function overlap of the initial bound state with the outgoing plane wave is expected to be small, and the process will be quasi-forbidden. A detailed calculation by Le Tourneux[24] has shown that the single-nucleon absorption rate is several orders of magnitude smaller than the observed total absorption rate, confirming that the single-nucleon process is indeed insignificant.

Absorption by two nucleons, hypothesized by Perkins,[25] eliminates the requirement for very high momentum components in the nucleon bound-state wave function. Brueckner, Serber, and Watson[26] recognized that such absorption requires a certain degree of correlation between nucleon pairs which permits them to be emitted simultaneously. To see this, consider two nucleons sharing the available energy of 140 MeV and emerging with a relative momentum of about 740 MeV/c. From uncertainty principle arguments, the absorption process must have involved relative distances of the order of 0.5 F. This is a small distance compared to the average internucleon spacing in C^{12} of about 2.5 F and is, in fact, comparable to estimates[27] of 0.4 F for the radius of the repulsive hard core. Extending these considerations one can argue that pion capture on three or more nucleons should be rare because of the small probability of finding such highly correlated aggregates in the nuclear volume. Supporting the model of pion capture by correlated pairs are the relative success of the phenomenological theories[28,29] based on this model and the observed[30] high probability of two-nucleon emission at about 180°. Consequently, absorption on correlated pairs has been an explicit assumption of all recent theoretical descriptions of pion interactions in complex nuclei. All of these theories seek to describe the

absorptive behavior of pions in nuclei in terms of either the fundamental π-nucleon interaction or (the inverse of) pion production cross sections. Presumably the only unknowns in such calculations are the nature of the nucleon pair correlations and the spatial distribution of nucleons in nuclei. Thus, in principle, both approaches are capable of providing new information on these aspects of nuclear structure.

The field theoretical calculations[31] generally have used the nonrelativistic π-nucleon interaction Hamiltonian

$$H = \frac{f}{\mu} \left(\vec{\sigma} \cdot \vec{\nabla}_\pi - \frac{\mu}{M} \vec{\sigma} \cdot \vec{\nabla}_N \right) \vec{\tau} \cdot \vec{\phi} \qquad (2)$$

where f is the pion-nucleon coupling constant, μ is the meson mass, M is the nucleon mass, $\vec{\sigma}$ and $\vec{\tau}$ are the nucleon Pauli spin and isospin matrices, $\vec{\nabla}_\pi$ is the momentum operator which acts on only the pion field $\vec{\phi}$, and $\vec{\nabla}_N$ operates only on nucleon wave functions. The three components of $\vec{\tau}$

$$\tau_1 = \begin{pmatrix} 0 & 1 \\ 1 & 0 \end{pmatrix} \qquad \tau_2 = \begin{pmatrix} 0 & -i \\ i & 0 \end{pmatrix} \qquad \tau_3 = \begin{pmatrix} 1 & 0 \\ 0 & -1 \end{pmatrix}$$

contracted with the three components of the pion field ϕ_1, ϕ_2, and ϕ_3 where

$$\frac{1}{\sqrt{2}} (\phi_1 \pm i\phi_2) \rightarrow \pi^\pm \qquad \phi_3 \rightarrow \pi^\circ$$

results in a scalar in isospin space, insuring charge independence. The first term on the right hand side of Eq. (2) is obtained directly from the relativistic form for the interaction, and notably is the simplest form which couples the pseudoscalar pion field to the scalar nucleon wave functions to obtain a parity-conserving theory.[32] The second term

has been added to insure Galilean invariance, i.e., that the interaction depends only on the relative momentum between the pion and nucleon. It is also clear that the second term is required in order to have absorption from 1s pionic states. However, it is not mandatory that the two terms have the same coupling constant; this point has been discussed by Barnhill[33] and Cheon[34].

The interaction given by Eq. (2) couples the initial nucleon states, generally described by shell-model wave functions modified by phenomenological pair correlation functions, to the final states of the emitted pair. The object of these calculations has been to predict the angular distribution, energy distribution, and species of the emitted particles and by comparison with experiment obtain information about the mechanism of the capture reaction, initial-state pair correlations, initial nucleon momenta, and two-hole excitations in the residual nucleus.

Several authors have also predicted total absorption rates from pionic 2p states which can be directly compared to the results of the present work:

1) Cheon,[35] using the shell model to describe the ground-state wave function of C^{12}, a phenomenological pair correlation function, and plane-wave states for the emitted nucleons, obtains

$$\Gamma_{2p}(C^{12}) = 16 \times 10^{15}\ \text{sec}^{-1} = 10.2\ \text{eV} \qquad (3)$$

This result was relatively insensitive to the value of the pair correlation parameter which was determined by selecting

the best fit to the angular distribution data and the experimental ratio of the number of np pairs to nn pairs emitted.

2) Chung, Danos, and Huber[36] calculated the total absorption rates from the 1s and 2p pionic states in O^{16}. They assumed a Woods-Saxon potential for the nucleons in both the initial and final states. The interaction of the emitted nucleons with the residual nucleus was described by an optical potential (with the imaginary part set equal to zero). Their form for the correlation function, assumed to be the same for both the initial and final states, permitted interpretation of the correlation variable directly in terms of the momentum exchanged between the two nucleons involved in the capture process. They obtained a maximum total absorption rate

$$\Gamma_{2p}(O^{16}) \approx 3.5 \times 10^{15} \text{ sec}^{-1} = 2.3 \text{ eV} \qquad (4)$$

for a characteristic momentum exchange of about 300 MeV/c. They noted that an absorption process also involving two nucleons but in which one of the nucleons remains bound in the residual nucleus may have a rate comparable to (4), but detailed calculations had not yet been completed.

3) Elsaesser and Eisenberg[37] emphasized the importance of an accurate description of the wave functions for the emitted nucleons. The initial state was assumed adequately described by shell-model harmonic-oscillator wave functions modified by a correlation factor. Noting only a weak dependence on initial-state correlations in their formalism, they performed the

numerical calculations using pure shell-model wave functions. They obtained

$$\Gamma_{2p}(O^{16}) = 113.6 \times 10^{15}\ \text{sec}^{-1} = 75\ \text{eV} \qquad (5)$$

The two finite values for the correlation parameter for which they repeated part of the calculation both resulted in increased transition rates.

The large disparity between the predictions (4) and (5) and the fact that (3) is larger than (4) while the converse should be true is symptomatic of the complexity of these calculations. For example, it is still uncertain whether the high-momentum Fourier components required in the nucleon wave functions are provided predominantly by initial-state correlations or by final-state interactions.[38] Interactions of the emitted nucleons with the residual nucleus have generally been ignored but have recently been shown to be quite significant.[31,36,39] Also, the effects of s-wave charge-exchange rescattering[40] of the incident pion and the influence of low-lying excited states of the residual nucleus[36] are seldom considered. It is for these reasons that it is difficult to draw definite conclusions from the field-theoretical calculations at this time.

An alternate approach to an understanding of the π-nucleus interaction is the semi-phenomenological description of Krell and Ericson.[21] The energy levels of the π-mesic atom are assumed given by the eigenvalues of the Klein-Gordon equation ($\hbar = c = 1$)

$$\{\vec{\nabla}^2 + [(E-V_c)^2 - \bar{\mu}^2]\}\ \psi = 2\bar{\mu}V\psi \qquad (6)$$

where V_c is the Coulomb potential corrected for finite nuclear size and vacuum polarization; $\bar{\mu}$ is the reduced pion mass, ψ the bound-state pion wave function, and V the strong-interaction potential. The phenomenological approach is to write the potential V in such a way that it is completely specified by empirical data on elementary π-nucleon scattering and pion production cross sections. To accomplish this Ericson and Ericson[41] chose to describe the low energy scattering of pions on single nucleons i and correlated nucleon pairs i,j by the scattering amplitudes,

$$f_i^{(1)}(\vec{r}) = [b_0 + b_1 \vec{t}\cdot\vec{\tau}_i + (c_0 + c_1 \vec{t}\cdot\vec{\tau}_i)\vec{k}'\cdot\vec{k}]\delta(\vec{r}-\vec{r}_i) \quad (7a)$$

$$f_{ij}^{(2)}(\vec{r}) = [B_0 + C_0 \vec{k}'\cdot\vec{k}]\delta(\vec{r}_i-\vec{r}_j)\delta(\vec{r} - 1/2(\vec{r}_i+\vec{r}_j)) \quad (7b)$$

where we have retained only the most important terms in both $f_i^{(1)}(\vec{r})$ and $f_{ij}^{(2)}(\vec{r})$. The parameters b_0, b_1, c_0, c_1 are real constants which are linear combinations of the elementary π-nucleon s-wave scattering lengths and p-wave scattering volumes. Similarly B_0 and C_0 are complex constants linearly related to various amplitudes of the (π2N) system. The δ-functions in $\vec{r}$ approximate the short range of the interaction, and $\delta(\vec{r}_i-\vec{r}_j)$ insures that pion absorption occurs on correlated pairs. Furthermore $\vec{t}$ is the isospin of the pion, $\vec{k}'$ and $\vec{k}$ the pion final and initial momenta, while $\vec{\tau}_i$ is the nucleon isospin. Using Eq. (7a) to describe elastic scattering $\pi + N \rightarrow \pi + N$ and Eq. (7b) to describe pion production $p + p \rightarrow \pi^+ + D$ one obtains experimentally determined values for the constant parameters in the scattering amplitudes.

Next, using a multiple-scattering formalism, the Ericsons obtain an expression for the pion wave function $\psi(\vec{r})$ which is a sum of the

incident wave plus contributions from the scattered waves from all other nucleons in the nucleus. The latter contribution is in the form of an integral in which the integrand contains the scattering amplitudes Eqs. (7a,b) and a Green's function which satisfies the Klein-Gordon equation with a δ-function source term. By applying the Klein-Gordon operator to $\psi(\vec{r})$ they obtain an equation in which they can identify a potential V such that

$$2\bar{\mu}V = q(\vec{r}) - \vec{\nabla}\cdot\alpha(\vec{r})\vec{\nabla} \tag{8}$$

with[42]

$$q(\vec{r}) = -4\pi[p_1 b_0 \rho(\vec{r}) + p_1 b_1(\rho_n(\vec{r}) - \rho_p(\vec{r})) + ip_2 \mathrm{Im}B_0 \rho^2(\vec{r})] ,$$

$$\alpha(\vec{r}) = \alpha_0(\vec{r})[1 - \xi \frac{\alpha_0(\vec{r})}{3}]^{-1} ,$$

and

$$\alpha_0(\vec{r}) = -4\pi[p_1^{-1} C_0 \rho(\vec{r}) + ip_2^{-1} \mathrm{Im}C_0 \rho^2(\vec{r})]$$

Here $p_1 = (1 + \mu/M)$ and $p_2 = (1 + \mu/2M)$ are kinematical factors; $\rho_n(\vec{r})$, $\rho_p(\vec{r})$, and $\rho(\vec{r})$ are the average neutron, proton, and nucleon densities, respectively. The variable ξ is a correlation parameter which the formalism indicates should be unity in the limit of zero range for the nucleon pair correlations.

Equation (6) with the strong-interaction potential V given by Eq. (8) has been solved numerically by several authors[18,21,43] to obtain the shifts and widths of the lower energy levels in π-mesic atoms. In these studies the phenomenological constants in Eq. (8) were treated as parameters to be varied to obtain the best agreement with available mesic

x-ray data. These "best fit" values for the parameters were then compared to those based on experimental data for π-nucleon scattering lengths and pion production cross sections. Before a valid comparison is possible the real parameters obtained from the elementary interactions must be adjusted for the specifically nuclear effects of finite correlation length and Fermi motion as well as the dispersive effects of pion absorption. The absorptive parameters must be adjusted to include absorption on nucleon pairs in a relative-singlet state. These corrections are discussed in detail in Ref. 21 and 41.

The energy level shifts in the π-mesic atoms are found to be well described by this model, and the parameters of the potential are in very good agreement with those based on elementary π-nucleon elastic scattering data.

The pionic 1s-level widths are not well described[21,29] in that the predicted dependence on nuclear charge is in disagreement with experiment for elements with $Z > 6$. Also, the experimental width in O^{18} is larger than that of O^{16}, whereas the theoretical isospin dependence should produce the opposite effect. Furthermore, the "best fit" value (including corrections) for ImB_0, the parameter determined almost exclusively by these widths, is larger by a factor of 2.5 that that obtained from pion production cross section data. On the other hand, this model is somewhat more successful in describing the 2p-level widths in pionic atoms; this will be discussed in detail in Sec. VI.

It is to be expected perhaps that the present model may not adequately describe the absorption of pions in complex nuclei. The implicit assumption that the initial and final-state correlations between

the absorbing nucleons in a nucleus are the same as those between the nucleons in the elementary pion production reaction is an oversimplification. Furthermore, the possible influence of final-state interactions between the emitted nucleons and the residual nucleus has not been included, nor have effects of nuclear excitations. Both of these phenomena were found to be significant in the field-theoretical calculations discussed earlier. Also, an interesting feature of the numerical analysis is that the "best fit" value for ImB_0 is most strongly influenced by the measured widths in elements with $Z < 7$. This results from the fact that these measurements represent the majority of the most precisely determined experimental data. The application of an optical potential to these low-Z elements with the anticipation that the parameters thus determined apply at higher Z may be naive. It is possible that the apparent "leveling off" of the 1s-level widths for $Z > 9$ could be conversely interpreted as an enhancement of the absorption rate in low-Z elements. This possibility will be further discussed in Sec. VI.

III. EXPERIMENT

The mesic x rays were observed in two experiments performed at the N.A.S.A. Space Radiation Effects Laboratory 600 MeV synchrocyclotron. Because the two experiments employed nearly identical beams, counter configurations, and electronics, only the first will be described in detail and the relevant differences noted.

A low duty-factor beam of negative pions was obtained by proton bombardment of an internal, vibrating beryllium target. Pions emerging from the thin vacuum window of the cyclotron were focussed by a pair of quadrupole magnets and transported in a He atmosphere to a bending magnet outside the cyclotron vault. The 190 MeV/c beam was deflected 35° by the magnet and traveled 2.4m in air through a 0.2m x 0.2m lead-lined aperture in an exterior shielding wall before arriving at the counter telescope.

A drawing of the scintillation-counter array and target-detector geometry is shown in Fig. 1. The degrader upstream of counter 1 was used only during the muonic x-ray runs. Electron rejection was accomplished by $\check{C}$, a Čerenkov counter filled with FC-75 viewed by two RCA 8575 photomultipliers whose outputs were summed in a logical OR mode. Counter 3 was employed to suppress the accidentals which would otherwise occur when neutrals from pion interactions in the degrader are detected by counter 4. Counter 7 served as a monitor of particles which might be scattered through large angles after entering the target, and counter 6 was used to monitor the efficiency of the veto counters $\check{C}$ and 5 as given by

$$\eta_{\check{C}5} = 1 - \frac{1\ 2\ \overline{\check{C}}\ 3\ 4\ \overline{5}\ 6}{1\ 2\ 3\ 4\ 6} \ . \qquad (9)$$

This quantity was generally in the range 0.95-1.00 depending on beam composition and whether the target was in or out of the beam. The efficiency $\eta_{\bar{C}5}$ and its use in determining the absolute number of meson stops will be discussed in more detail in Sec. IV.C. All counters were square with the exception of the target-defining counter 4 which was a 3" (diam.) x 0.063" disk of scintillant mounted in a 4" x 4" x 1/8" Lucite support. In the second experimental run counter 7 was eliminated, counter 5 was inclined more toward the beam axis, and a 5" x 5" x 1/8" veto counter was placed against the downstream face of the target. In both experiments the target-detector axis was perpendicular to the target plane and 45° to the beam axis. The targets were held in a fixed position relative to the detectors by a rigid frame mounted on the detector cryostats. Counter 4 could be translated a short distance along the beam axis to accommodate targets of different thickness and remain in contact with the upstream face of the target.

A block diagram of the electronics is shown in Fig. 2. Many of the components were used only as performance monitors and were not used in establishing the prompt time signature for a stopping particle which was $1\ 2\ \bar{\check{C}}\ 3\ 4\ \bar{5}\ \bar{7}$. Figure 3 shows a range curve obtained in a 3.2 g/cm^2 carbon target with this signature. In addition to the prompt time signature a pulse-height restriction was placed on the amplitude of the pulse in counter 4 to reject events which occur when the pion stops in 4 rather than in the target. This was found to be feasible because the signal generated in the scintillant by a stopped pion ("star" event) was usually detectably greater than that from a slow pion transversing the entire thickness of the scintillant. The pulse height from

the 14th dynode of the 56AVP photomultiplier on counter 4 was analysed to determine the threshold on discriminator D4'. This technique was approximately 60% effective for discriminating against pion stops in counter 4 and was shown to produce a negligible "dead-layer" on the upstream surface of the target. The complete stops signature was then

$$1\ 2\ \bar{\check{C}}\ 3\ 4\ \bar{4}'\ \bar{5}\ \bar{7}\ . \qquad (10)$$

The consequent reduction of the mesic x-ray background from carbon in the Li^6 spectrum simplified the analysis appreciably. The spectra of the other targets were relatively unaffected, and the technique was not used in the second experiment which concentrated on elements $6 \leq Z \leq 22$.

All targets except $(H_2)O^{16}$ consisted of one or more thin plates which facilitated measurement of x-ray absorption coefficients to be used in the self-absorption corrections. When the effects of impurities and target coverings were included, all measured absorption coefficients were consistent with those in published compilations.[44] A summary of target properties and some typical rates using the complete signature for a stopping particle are given in Table I.

The solid-state detectors used to detect the x rays are listed along with their relevant physical and electronic characteristics in Table II. All detectors were operated at liquid nitrogen temperatures and employed cooled field-effect transistors as the first stage of amplification.[45] Subsequent amplification and pulse shaping were performed with Tennelec TC201 and TC200 amplifiers. The planar Ge(Li) detector system employed a pole-zero modification to the main amplifier. The coaxial Ge(Li) detector spectrometer included an Ortec 438 base-line

restorer. The shaped pulses were analysed and stored by a Victoreen SCIPP 1600 channel pulse-height analyzer (PHA) which was gated whenever a signal in the x-ray detector coincided with a meson-stop signature. To establish this coincidence a zero-crossing technique was employed to obtain a timing pulse from the detector signal. The block diagram in Fig. 2 shows the Canberra 1410 double-delay-line amplifier (DDLA) which produces a zero-crossing signal from an unshaped detector pulse obtained from an electrically isolated output of the main amplifier. The energy window of the Ortec 420 single-channel timing analyser (SCTA) accepted signals only in the energy range of interest in order to minimize count-rate effects.

A plot of the number of these x-ray timing signals versus the time at which they occur relative to a meson-stop signature exhibits a prominent peak on a flat background. This "timing peak" resulting from the correlation between meson stop and x-ray emission was continuously monitored on a second pulse-height analyser which displayed the output of a time-to-amplitude converter (TAC) (see Fig. 2).[48] The sum of the widths of the output pulses of discriminators D 11 (x ray) and D 10 (meson stop) determined the timing window within which an x-ray signal was said to coincide with a meson stop. This window was 320 nsec wide for all detectors and was centered on the timing peak. Figure 4 shows a typical timing spectrum with the window containing the "good" events stored in a separate section of the analyser to facilitate monitoring the performance. The timing window included part of the "flat" background in the prompt timing to preclude loss of very low energy pulses due to possible energy-dependent time shifts.

The data acquisition procedures were essentially the same for all targets. First, the degrader thickness was adjusted to obtain a maximum rate of pion stops. Standard sources[49] which emitted γ rays or x rays whose energies covered the region of interest were attached to the center of the downstream face (detector side) of the target, and data from these sources were accumulated for a fixed "live" time with the beam on. During these absolute efficiency measurements the gate for the x-ray PHA was generated by the x-ray timing signal alone, the meson-stop signature requirement at C9 (Fig. 2) having been removed. Analysis of the detector efficiency data will be discussed in Sec. IV.B. Following the calibrations, the sources were removed, the meson-stop signature requirement was reinstated, and mesic x-ray data were accumulated. After the pionic data were recorded, sufficient degrader material was added to maximize the rate of muon stops, and the procedure was repeated.

At the conclusion of the muonic x-ray run the target was removed, and target-out beam rates were established for both the muon and pion beams. The use of these rates in determining the absolute number of stopped mesons will be discussed in Sec. IV.C.

IV. ABSOLUTE YIELD MEASUREMENTS

A. Analysis of Spectra

Peaks in the mesic x-ray spectra were analyzed primarily to determine the number of x rays corresponding to the transitions of interest and the uncertainties to be assigned to those numbers. The energies and, where applicable, the strong-interaction broadening of the transitions were determined and compared to the more precise values which have appeared in the literature.[18,46,50,51] The agreement was generally good, and discrepancies were always within the estimated uncertainties in the present measurements. Two specific examples will be discussed in Sec. IV.D.

The major contribution to the uncertainty in the number of counts in a given x-ray peak arose from the uncertainty in the background. The use of thin, small targets, while reducing the importance of possible systematic errors, limited the statistics which could be accumulated in a given amount of running time. Although the relatively low statistics occasionally aggravated the problem of determining the characteristics of the background, in most instances improved statistics would not have significantly reduced the uncertainty of the final result. In this sense the analysis generally was not limited by statistics. Another complication was the asymmetry of the peaks obtained with the coaxial detector. Because the asymmetry was observed to be essentially independent of the amplification system, employing consistent criteria in

analyzing calibration spectra and mesic x-ray spectra assured that systematic uncertainties would largely cancel. As a consistency check, the L-series in Mg and the K-series in C were investigated using both Ge(Li) detectors, and the final results were found to be in good agreement. The most significant systematic uncertainties in the background were due to the presence of contaminant peaks, generally defined as any peaks not belonging to the mesic x-ray series of primary interest. In the present experiment contaminant peaks could have arisen from the following phenomena:

1) the presence of muons in the pion beam. With the degrader thickness chosen to maximize the rate of stopping pions in the target the ratio of muon to pion stops was of order 1:10. However, for the K-series the muonic x-ray yield is always significantly larger than the pionic x-ray yield, and the muonic lines actually dominate the spectra for $Z \geq 6$. In the present experiment the muonic x-ray peaks were the major contaminants in the pionic spectra of Be, C, and O as can be seen in Fig. 5.
2) mesons stopping in any material other than the target. Such events are inconsequential unless they coincide with a meson-stop signature. Hence, most events of this type occurred when the meson stopped in any non-target material between (and including) counter 4 and the scintillant of counter 5. Because carbon was the most abundant element in these materials, its x rays appeared in most spectra and in particular complicated the interpretation of some of the Li, C, and Mg data. In some instances small contaminant peaks due to mesons which had been scattered into the detector cryostat were also observed.

3) the decay of nuclear excited states following nuclear pion capture in the target. The time interval between a pion stop and the appearance of a de-excitation nuclear γ ray is usually very short compared to the timing-window width of 320 nsec. Hence they cannot be discriminated against by the electronics and may appear in the mesic x-ray spectra. In Fig. 5(c) four such contaminant peaks in the pionic oxygen spectrum are indicated.

Other phenomena which might have produced background peaks were investigated and found to be of little or no significance. These included flouresence effects which might produce atomic x rays in the cryostat or shielding materials, pion contamination in the muon beam, and nuclear muon capture.

In an attempt to locate and identify all significant contaminant peaks and thus reduce the uncertainties in the background, the spectra were subjected to three separate examinations:

a) all spectra were "scanned" by computer-fitting each identifiable peak in a spectrum to a Gaussian function plus a linear background, the number of data channels included in the fit being as large as practicable. Groups of adjacent data channels were then summed to enhance peaks of smaller amplitude which were otherwise obscured, and the peaks were fitted again. In this way all peaks were tentatively identified and catalogued.

b) portions of spectra containing peaks separated by less than approximately 4Γ (Γ is the full width at half maximum of the

broadest peak in the spectrum) were decomposed by obtaining a fit to a two-Gaussian function plus linear background. If the contaminant in a pionic x-ray spectrum consisted of a muonic x-ray series it was usually possible to subtract the entire series using a clean muonic x-ray peak in the pionic spectrum as a reference; this reference peak was compared to the corresponding peak in a muonic spectrum taken with the pure muon beam to obtain a scale factor; the scaled muonic x-ray spectrum was then subtracted from the pionic spectrum. After the separated peaks were examined for anomalies which the adjacent peaks might have concealed, those exhibiting natural broadening were fitted to Voigt profiles[52] and all others were fitted to Gaussians. In all cases the interval of the fit was approximately 4Γ and centered on the peak.

c) plots of spectra (usually with groups of adjacent data channels summed) were examined and the subtraction of contaminant peaks and linear background was performed by eye.

For most x-ray transitions of interest both (b) and (c) were employed to obtain the number of counts (detected x rays) in the peak and as a rule gave consistent results. This general agreement was felt to justify using the results of (c) alone in those few instances when very low statistics made application of (a) and (b) impractical. Whenever (b) and (c) produced different results, the discrepancy never exceeded 2.0 standard deviations and was usually less than 1.5. In all such cases the spectra were re-examined, possible causes of the discrepancy established, and a final number selected with an assigned uncertainty larger than either of the original uncertainties.

The analysis of the carbon data required special techniques because of the relative abundance of carbon in non-target materials such as scintillants, counter wrappings, and degraders. The observation of carbon L-series x rays in the Li and Be spectra and their absence in the Mg spectra strongly suggested that all carbon contamination originated upstream of the target.[53] Subsequent detailed analyses of the intensities of the carbon x-ray peaks which appeared in many of the spectra were consistent with the hypothesis that all of these x rays originated in the scintillant of counter 4. The contribution from counter 4 either could be subtracted from the carbon x-ray spectra or it could be included and the target volume and number of meson stops adjusted to include the counter. The latter technique was the one employed and resulted in approximately a 10% correction to the total number of stops.

B. Detector Efficiencies

The absolute net efficiencies of the three detectors were determined over energy ranges which spanned the mesic x-ray spectra of interest. The absolute net efficiency is defined here as

$$\frac{\text{no. counts in full-energy peak with source at distance D}}{\text{no. } \gamma \text{ rays emitted}},$$

where the source was on the symmetry axis of the detector. The distance D is given in Table II. The number of γ rays was determined from the calibration data provided by the supplier[54] and corrected for absorption in the source holders. Hereafter the use of the word <u>efficiency</u> shall mean the absolute net efficiency as defined above.

The efficiencies at energies for which calibrated sources were available were plotted versus energy on logarithmic graphs and the points connected by a smooth curve. The final results are shown in Fig. 6. Knowledge of the shapes of the Ge(Li) detectors' efficiency curves was improved by employing an uncalibrated Ba^{133} source. The Ba^{133} spectrum contains several γ rays whose relative intensities are well known[55] and whose energies are within the range spanned by the Ge(Li) detectors. The relative efficiency data obtained with the Ba^{133} source were normalized to the absolute efficiency data by equating the efficiency at 279 keV (Ba^{133}) to the absolute efficiency at 276 keV (Hg^{203}, calibrated[49]).

A counterpart to the Ba^{133} source which would have aided in determining the shape of the Si(Li) efficiency curve was not available. The alternative technique used was to determine a theoretical efficiency curve from a knowledge of the physical components of the system and the appropriate photon absorption coefficients. The theoretical relative efficiency curve was superimposed on the experimental data points obtained from calibrated sources by normalizing at 14.4 keV. Two of the experimental points are inconsistent with the predicted curve shape and require further comment. They are the 18-keV and 21-keV L_β and L_γ x rays of Np^{237} produced by the alpha decay of Am^{241}. The absolute intensities of these x rays have been measured elsewhere[56] using an argon proportional chamber spectrometer which resolved only the most prominent peaks. A more recent investigation[57] in which these intensities were used to calibrate a Si(Li) detector spectrometer indicated that the intensity of the 18-keV series may be greater than that given in Ref. 56.

In the present experiment the spectrometer resolution was better than those in Ref. 56 and Ref. 57, perhaps permitting more accurate determination of the background, which may account for the discrepancy at 21 keV as well as at 18 keV. The possibility of a systematic uncertainty in the background combined with the fact that no alteration in the parameters for the theoretical shape could provide agreement at these two points without destroying the agreement at all other points was the basis for rejecting the quoted Np^{237} x-ray data at 18 keV and 21 keV.

Having determined the efficiency of the detectors to a point source located on the symmetry axis of the detectors, we measured the efficiency off-axis relative to the efficiency on-axis to find the uniformity

$$U(r,\phi,D) = \eta(r,\phi,D)/\eta(r=0,D)$$

where $\eta(r,\phi,D)$ is the absolute efficiency of the system to a source at the location specified, and the origin of the cylindrical co-ordinate system is taken at the center of the front surface of the detector. These uniformity measurements were made over an area somewhat larger than the size of the target and repeated at several different energies. The average of $UD^2/(r^2+D^2)$ over the target area was approximately 0.95 for both the Si(Li) detector and planar Ge(Li) detector and 0.90 for the coaxial Ge(Li) detector.

Knowledge of U made off-axis efficiency measurements during the mesic x-ray runs unnecessary, and prior determination of the shapes of the efficiency curves permitted the use of only a few sources to establish the absolute efficiency over a wide range of energies. Thus,

the frequent calibrations referred to in Sec. III did not require an inordinate amount of time.

The detector efficiencies *in situ* were obtained from the beam-on efficiency measurements described in Sec. III. These measurements were compared to those taken with the beam off as well as to measurements taken earlier in the laboratory. The data taken with the beam off were in very good agreement with the earlier measurements. Analysis of the beam-on results indicated beam-dependent deadtimes which, though different for each detector, were essentially independent of both energy and target material.[58] The deadtime, attributed to the effect of overload pulses on the amplifiers and not to conventional count-rate effects, reduced the efficiency of the planar Ge(Li) detector by approximately 22% and 10% during the pionic and muonic x-ray measurements respectively. The deadtime in the other two detectors were approximately half of that in the planar Ge(Li) detector.

To determine the efficiency for any given energy generally required interpolation between two calibration points which bracketed the energy region of interest. Occasionally extrapolation was necessary and resulted in the assignment of somewhat larger uncertainties to the absolute efficiency. Both techniques utilized the curve shapes shown in Fig. 6. The one exception was the determination of the Si(Li) detector efficiency at 6.1 keV (muonic 3d-2p line in Be^9). Below approximately 7.5 keV the Si(Li) detector deadtime was no longer independent of energy but increased rapidly with decreasing energy. This effect was not recognized until after the experiment had been completed, and the available data did not permit a thorough investigation

of the phenomenon. Nonetheless, it was possible to determine the effect on the detector efficiency during the calibration run by comparing the low energy (Compton) background in spectra obtained with the beam on and with it off. The attenuation at these low energies which was quite apparent in the calibration spectrum appeared to be less severe in the mesic x-ray spectrum. The difficulty in specifying the efficiency in this low energy region is the principal cause for the large uncertainty assigned to the yield for the L_{α}^{μ} line in Be.

C. Determination of the Number of Stopping Mesons

The total number of pions and muons stopping in the target during an x-ray run was taken to be the scaled number of stop signatures (10)

$$12\check{C}34\bar{4}'\bar{5}\bar{7}$$

corrected for veto-counter efficiency, outscattering, and events satisfying (10) but occurring in materials other than the target. This last correction was obtained by measuring the stopping rate (with respect to 1234 events) with the target removed and multiplying this rate by the number of 1234 events during the x-ray run. This product, corrected for the efficiency of the veto counters and outscattering, was the total number of stops occurring in non-target materials. Implicit in this computation was the assumption that the stopping rates in these materials did not change when the target was removed. This assumption was justified for the following reason. Because the stopping rates in any given material are affected only by the degrader upstream, clearly

all rates in materials upstream of the target are independent of the target. For materials downstream of the target the target-in and target-out stopping rates will be very nearly the same if the distribution of stopping mesons is symmetrical about its maximum and is centered in a target which is relatively thin. These conditions were assured through the use of thin targets (see Table I.) and by adjusting the degrader thickness for each target to obtain a maximum stopping rate. The symmetry was confirmed by inspection of the range curve (Fig. 3). Typically less than 15% of the stop signatures corresponded to events occurring in non-target materials.

The veto-counter efficiency (9) as determined using counter 6 was by definition a relative number which depended on the composition of the beam passing through veto counter 5. Because 5 was less sensitive to electrons than to muons or pions and the Čerenkov counter was not perfectly efficient, the higher the proportion of electrons in the beam the lower the efficiency. Thus we observed $\eta_{\check{C}5} \approx 1.00$ for target-out runs in the pion beam and $\eta_{\check{C}5} \approx 0.95$ for target-in runs in the muon beam. The exact values for each run were used to correct the corresponding numbers of total stops.

Counter 7 intercepted some of the particles which emerged from the target at large angles and missed counter 5. Because it was anticipated that such outscattering would be only a small correction to the stopping rates, no effort was made to examine it in detail. We assumed that the outscattering would be cylindrically symmetric about the beam axis and that we could ignore scattering through angles greater than approximately 90° in the laboratory frame of reference. The number

of false stop signatures which counter 7 prevented was taken to be the number of counts registered in C4 minus those registered in C5 (see Fig. 2). Had counter 7 completely encircled the beam at the same distance from the beam and with the same extent along the beam axis, it would have covered a solid angle 6.2 times larger. The preliminary outscattering correction was, therefore, 6.2 x (C4-C5) and amounted to typically a 3% effect in the pion stopping rates and less than a 1% effect in the muon stopping rates. By taking into consideration the interaction of neutral secondaries (to be discussed in the next paragraph) in counter 7 the outscattering effect was found to be reduced to generally less than 2% and 1/2% in the pion and muon cases respectively. In the second run, the veto counters were much closer to the target and corrections for outscattering were ignored.

A non-negligible correction to the veto-counter efficiency as well as to the outscattering contribution arises from the interaction of beam-associated neutrals in counters 6 and 7. The neutrals include mesic x rays, meson-capture γ rays, neutrons, and nuclear γ rays, and clearly there may be several associated with each stopped meson. With the assumption that there are no neutrals emitted when the target is out, i.e., all counts accumulated at C7 represent "true accidentals", the number of detected neutrals is given by

$$(C7)_{\text{Target In}} - (C7/C2)_{\text{Target Out}} \times (C2)_{\text{Target In}}$$

The number of detected neutrals per meson stop were a factor of 3 or 4 greater in the pion runs than in the muon runs. Data from typical pion runs indicated approximately three emitted neutrals per stop if the

average intrinsic detection efficiency is 2%. By including both the effect of neutrals and outscattering, the stopping rates were altered by at most 2%.

Applying the above corrections to the counted number of stop signatures, we obtained the total number of stops in the target. It remained to determine the pion contamination in the muon runs and the muon contamination in the pion runs. From range-curve analyses and searches for pionic x-ray peaks in muonic x-ray spectra[59] we concluded that the muon beam was free of pion contamination.

According to range-curve analyses, the stopping-pion beams in the two runs contained respectively about 6% and 9% muon contamination while investigation of muonic x-ray peaks in the pionic x-ray spectra indicated contaminations ranging from 2.5% to 5% in the first run and 2.5% to 7% in the second run. The generally large uncertainties associated with these numbers do not entirely exclude possible systematic differences between targets. Because of this difficulty the most probable value for the contamination was selected, and it was assumed the same for all targets in the run. The values used for the two runs were $(3.5 \pm 1.0)\%$ and $(5.0 \pm 2.0)\%$ respectively. It should be noted that these uncertainties in the muon contamination contribute less than 2% to the uncertainties in the final values for the absolute yields.

The distributions of stopping mesons in the direction of the beam axis were assumed to coincide with the shapes of the peaks in the range curves. Near their maxima the peak shapes were very nearly Gaussian which simplified computation. Uniformity over the target plane, which was assumed in all calculations, was virtually assured by

the small size of the targets. This assumption was not critical because the symmetry of the target-detector geometry insured that final yield values would have a negligible dependence on the distribution in the target plane.

D. Pionic and Muonic X-Ray Yields

The absolute and relative yields of all observed transitions were computed by dividing the disc-shaped targets into small annular elements, calculating the contribution for each element assuming isotropic x-ray emission,[60] then integrating over the target volume. The number of axial increments was chosen to insure that the x rays were attenuated less than 1% in traversing one incremental thickness. The results of the calculation were essentially independent of the number of radial increments, which was selected to be 30 for all targets. These calculations were performed by computer which facilitated investigating perturbations such as different meson-stop distributions and enlarged effective target volumes due to the divergence of the beam. Their contributions to the total uncertainties in the yields were found to be negligible. The final yield values are presented in Tables III and V where they are compared with previously published results. The calculated values in Table III will be discussed in Sec. V.

The muonic x-ray yields were measured to investigate systematic errors which might have arisen either in the experiments or in the data analysis. The K-series is particularly useful for this purpose since it is generally accepted that the total series yield is very nearly unity in all elements with the probable exception of Li. The pionic and muonic

L-series x-ray yields were measured also for Mg and Ti since these x-rays bracket in energy the K-series of C and O. The yields obtained for these "reference" lines are generally in good agreement with earlier work and with the predictions of the cascade calculations (Sec. V).

The lack of agreement between the present result for the pionic 2p-1s yield in C and that of other experimenters may be due in part to the difficulty of subtracting the muonic background from the pionic x-ray peak. The muonic np→1s x rays ($n \geq 3$) all fall in the energy range spanned by the broadened pionic K_α peak and have a yield approximately a factor of ten higher. Thus with a 5% muon contamination of the pion beam one-third of the "signal" in the region of the pionic K_α line will consist of muonic x rays. The subtraction of these contaminant peaks, therefore, requires particular care since the result may strongly influence the measured characteristics of the pionic line. In the present analysis two different techniques were used. Because the data from the first experimental run contained some pionic x rays in aluminum (detector cryostat) on the low energy side of the C pionic K_α peak, the peak was analysed only on the high energy side of the centroid and the uncertainty in the final result was increased to reflect the uncertainty in the centroid location. In the second experimental run the detector cryostat was farther from the beam and no x rays from Al were evident; the entire muonic K-series could then be subtracted from the pionic spectrum using the technique described in Sec. IV.A. The yields thus obtained in the two experiments were consistent within approximately one standard deviation. The natural broadening of the pionic K_α line was determined to be approximately 3.2 keV and 2.7 keV in the two

experiments with the latter exhibiting the larger yield, as might occur for incomplete subtraction of the muonic background. We conclude that with muon contamination of the pion beam of the order of 5% it is unlikely that differences in background-subtraction techniques could contribute an uncertainty larger than the 15% found in the present case.

The oxygen pionic K_α x ray is contaminated by two nuclear γ rays in addition to the muonic x rays. Subtracting the entire muonic K-series from the pionic spectrum (see Sec. IV.A) produced a much less cluttered spectrum in which the nuclear γ rays were clearly resolved and easily subtracted by eye. In comparing the yield obtained in the present investigation with those of earlier investigators the differences in apparatus and techniques should be noted. In particular the experiments of Camac et al.[62] and Stearns et al.[5] employed NaI(Tl) crystals whose energy resolution was incapable of resolving the nuclear γ rays and muonic x rays just discussed. The γ rays alone constitute approximately 15% of the "signal" in the vicinity of the pionic K_α peak. The analysis is further complicated if the two unidentified γ rays near the expected location of the K_β peak are also target-associated.

With regard to muonic x-ray background Stearns et al.[5] did not discuss any corrections to their data for possible muon contamination in their pion beam. Camac et al.[62] deduced 1% muon contamination from their oxygen data and 1.5% from the nitrogen data but were unable to make determinations of contamination from the data for their other targets; for all targets except nitrogen they assumed a 1% muon contamination. More recently, Koch et al.[19] using a high resolution Ge(Li) detector were able to compare accurately the intensities of the muonic x rays

and pionic x rays in their pionic spectra. Knowing the absolute yields of the (K-series) muonic x rays and assuming the muon contamination in the pion beam to be the same as that measured in two reference targets, they were able to calculate the absolute yields of the pionic x rays. Unlike the results of the present experiment, the absolute yields obtained using this technique are very sensitive to uncertainties in the ratio of muon to pion stops in the target. There exists evidence in the present work (see Sec. IV.C) and that of Ref. 62 which suggests the possibility of different muon contamination for different targets. While such a phenomenon seems very improbable, it could introduce systematic errors in any analysis which used muonic x-ray lines as intensity references and assumed a muon contamination in the pion beam which was independent of target.

V. ATOMIC CASCADE AND NUCLEAR ABSORPTION

The level populations $P_{n\ell}$ to be used in Eq. (1a) were deduced from the absolute yields measured in this experiment. To accomplish this a calculation of the atomic cascade scheme was performed which predicted mesic x-ray yields on the basis of assumed values for the $P_{n\ell}$. In general, yield data were available for a sufficient number of x-ray transitions in each element to permit an unambiguous determination of all level populations in the cascade scheme.

A. Description of the Cascade Calculations

The cascade calculations[64] are nearly identical to those done by Eisenberg and Kessler[12-14] and by Koch et al.[19,20] At the beginning of a calculation the initial population of the angular momentum states of a high n level is assumed. The electromagnetic transition rates are calculated using the expressions given by de Borde[65] and Burbidge and de Borde[66] for Auger emission of K and L-shell electrons and for E1 radiative transitions. For the calculation of these rates it is assumed that all bound states are adequately described by hydrogenic wave functions (pionic 1s and 2p states which are exceptions will be discussed later). In the present work an approximation is used in which the state of each particle in the mesic atom is characterized by Z_{eff}(field) and Z_{eff}(potential), where Z_{eff}(field) is the effective charge which appears in the wave function, and Z_{eff}(potential) is used to calculate the binding energy or transition energy. The difference between

Z_{eff}(potential) and Z_{eff}(field) is the "outer screening" contribution discussed by Slater.[67]

In the calculation of the effective charge the meson is assumed to be screened by only the K-shell electrons, an excellent approximation for mesic levels with $n \lesssim 20$. Hydrogenic wave functions are used for the electrons, and the meson is assumed to be localized at the Bohr radius

$$r_n = \frac{\hbar^2}{\bar{\mu} e^2} \frac{n^2}{Z_{eff}(\text{field})}$$

where $\bar{\mu}$ is the meson reduced mass.[68]

The electrons are screened by the other electrons in the atom as well as by the meson. Electron screening was computed using a technique very similar to Slater's simplified treatment of ionization potentials in light atoms.[69] The screening of the electrons by the meson was estimated by ascribing to all particles wave functions with maxima at their Bohr radii and Gaussian radial distributions about these maxima. Reasonable variations in the parameters used in the screening calculations were found to have an insignificant effect on the final results of the cascade calculations. The results of the screening calculations for the muonic carbon atom are shown in Fig. 7.

The nuclear absorption rates from the 1s, 2p and 3d states of the pionic atoms were treated as variables even though for most elements the results of the calculation were sensitive to only one of these three parameters. Absorption rates from higher n levels were obtained by multiplying these rates by scaling factors $R(n\ell/n'\ell)$ which were the ratios

of the overlap of the square of the pion wave functions with the nuclear volume. Using hydrogenic wave functions[70] for the pion states, we obtained to first order

$$R(ns/1s) = \frac{1}{n^3}$$

$$R(np/2p) = \frac{32}{3}\left(\frac{1}{n^3}\left(1 - \frac{1}{n^2}\right)\right) \qquad (11)$$

$$R(nd/3d) = \frac{2187}{40}\ \frac{1}{n^3}\left(1 - \frac{5}{n^5} + \frac{4}{n^7}\right) .$$

In the approximation that the pionic wave functions for states with $\ell > 0$ are proportional to r inside the nuclear volume, one obtains the same expressions as above for the ratios of the squares of the wave functions at the nuclear surface or the squares of the gradients of the wavefunctions integrated over the nuclear volume. Thus Eqs. (11) are largely independent of the nature (e.g., local or non-local) of the absorptive interaction. For the elements investigated in the present work, absorption from states with $\ell > 2$ is negligible and has been ignored.

B. Choice of Initial Level

In the cascade calculation one varies the initial distribution of mesons in the higher states and, in the pion cascade, the nuclear capture rates to obtain the experimental x-ray yields. The cascade parameters, thus selected, uniquely determine the populations $P_{n\ell}$ of the lower levels of the mesic atom. Using the cascade calculation in this manner is the equivalent of applying Eq. (1) self-consistently to all observed x-ray transitions in the mesic atom.

The initial distribution is established by specifying an initial level N and the relative populations $P_{N\ell}$ of the angular momentum states in that level. Because the only constraint on $P_{N\ell}$ is that the cascade calculation reproduce the experimental yields, the choice of N is clearly somewhat arbitrary. Economy of effort would seem to indicate that the calculation should begin at the lowest value of N that is physically reasonable, for example, one not much higher than that of the highest initial level of an observed x-ray transition. In the present experiment this level is n = 6 corresponding to the observed L_δ and M_γ transitions in magnesium. Because it was estimated that unresolved, very low intensity x rays may have originated from as high as n = 8, it was decided to begin the cascade at n = 9. The argument could be made that to begin the cascade calculation at a somewhat higher level, while having an insignificant effect on the deduced populations of the lower levels, would produce more useful information about the cascade itself. However, the explicit assumptions of the cascade calculation become less valid for higher principal quantum numbers, and consequently the deduced initial distribution has less physical significance. For example, above n = 11 in muonic Li^6 a transition of $\Delta n = 1$ by Auger emission of a K-shell electron is energetically forbidden. As there are no L-shell electrons associated with this mesic atom, which behaves chemically like a He^6 impurity in a Li^6 lattice, these transitions must occur radiatively or by interaction with a conduction electron in the host lattice. This latter interaction is not computed in the cascade calculation. Also, in Be^9 and C^{12} the L-shell electrons are conduction electrons

better described by Bloch states than by hydrogenic wave functions; when interactions with these electrons are significant in the cascade process, the present calculation is clearly inadequate. In addition, electron screening becomes more important at higher n levels, significantly raising the states with large angular momentum. Sliding transitions ($\Delta n = 0$, $\Delta \ell = -1$) are then more probable but are not considered in the present calculation. Finally, there is evidence that in many substances large mesic molecules are formed, and the meson may not be bound to a particular atom until it arrives at a very low ($n \sim 7$) level.[71]

We conclude that "initial" distributions deduced with existing cascade calculations become increasingly suspect for levels much higher than $n \sim 9$, the actual upper limit depending on the nature of the target material, the accuracy desired, and the sophistication of the calculation. Thus if the primary object of the calculation is to obtain the populations of the lower atomic levels, beginning the cascade at high n appears unwarranted.

C. Results of the Cascade Calculation

The initial meson population of the angular momentum states in the $n = 9$ level was found generally to be adequately described by a modified statistical distribution

$$P_{9\ell} \propto (2\ell + 1)e^{a\ell} , \qquad (12)$$

where a is chosen such that the cascade calculation reproduces the experimental x-ray yields.

In the present cascade calculation the muonic 2s level in all elements is assumed metastable, decaying only by a $\Delta\ell = 0$, Auger transition.[11,65] However, in all elements except Li the total K-series muonic x-ray yield is consistent with unity, indicating either a 2s→2p transition or a mixing of 2s and 2p states. For $Z > 6$ the finite-nuclear-size effect sufficiently reduces the binding energy of the 2s state, and the 2s→2p transition is possible. However, in elements with $Z < 6$ the 2s state is lower in energy than the 2p state because of the effect of vacuum polarization.[11] For these elements Ruderman[11] has proposed a "mixed" Auger-radiative transition in which an atomic electron receives the one unit of angular momentum which must be transferred when the meson makes the virtual 2s↔2p transition. While it is in the 2p state, the meson may be thought of as being off its mass shell by an amount equal to the 2s-2p energy difference plus the excitation energy of the electron. The net rate for the transition 2s↔2p→1s is the normal 2p→1s radiative rate times the fraction of mixed-in 2p state. The emitted x ray has the energy of the normal 2p-1s x ray minus the amount by which the meson was off its mass shell while in the 2p state. For Be^9, if a K-shell electron were emitted, this energy difference would be about 60 eV which is very small compared to the K_α x-ray energy of 33.4 keV. On the basis of measured yields, it appears that this mixed transition completely depopulates the 2s states in Be, B, and C but is at best only partially effective in Li (see Table III and Ref. 15). This difference might be due in part to the presence of L-shell (conduction-band) electrons in mesic Be, B, and C atoms and their relative absence in mesic Li. Ruderman indicated that the omission of

L-shell electrons from his calculation probably resulted in an underestimate of the mixed-transition rate. Using his expression for the fraction of 2p mixing and hydrogenic wave functions for the L-shell electrons, one obtains only a small contribution to the mixing rate. However, it may be that the near-zero energy required to excite a conduction electron (a factor which enhances the mixed-transition rate) compensates sufficiently for the small wave function overlap of the conduction electrons with the meson so that a more exact analysis is required.

In the interpretation of the cascade calculations it was assumed that the total K-series muonic x-ray yields should be unity in all elements with $Z \geq 4$. Therefore, the predicted 2s-state population was added to the 2p-state population to obtain the total number of mesons which produce K_α x rays. For Li we used the estimated value[11] of 0.58 for that fraction of the 2s-state population which decays by the $\Delta\ell = 0$, radiationless Auger transition.

To determine the value of $\underline{a}$ in expression (12) that best describes the "initial" population, the yields predicted by the cascade calculation were compared to the experimental measurements. Relative yields, because of their smaller experimental uncertainties, generally were the most significant in determining $\underline{a}$. As illustrated in Fig. 8 for muons in C^{12}, the value $\underline{a} = +0.32 \pm 0.07$, which is the weighted average of $\underline{a}_1$, $\underline{a}_2$, $\underline{a}_3$, and $\underline{a}_4$, is seen to reproduce satisfactorily the experimental values. The results of this analysis for all muonic atoms are listed in Tables III and IV.

The pion-cascade calculations contained one variable in addition to $\underline{a}$: $\Gamma_{2p}(\text{cap})$ in Li^6, Be^9, C^{12} and O^{16}; $\Gamma_{3d}(\text{cap})$ in Mg and Ti. The capture rates from the other angular momentum states either have been directly measured or were extrapolated from direct measurements in higher-Z elements using wave function overlap arguments; large variations in these capture rates had negligible influence on yields predicted by the cascade calculations. These rates, expressed in terms of the widths of the corresponding states, are denoted by superscript (a) in the last three columns of Table VI.

Two techniques were used to select the "initial" population for the pion-cascade calculation. The first assumes that when the pion and muon have the same binding energy they have the same distribution among angular momentum states in their respective n levels. Because of the larger mass of the pion, it has approximately the same energy in the n = 11 level as a muon in n = 9; by the above assumption, the populations of the pionic and muonic angular momentum states in these levels may be described by the same value of $\underline{a}$. This method has been used by Backenstoss[18] who then assigns a 10% uncertainty to the population of the lower pionic levels to account for possible differences in the muon and pion cascades.[72]

The second technique is essentially identical to that described earlier for the muon cascade calculation. In pionic atoms certain yields are approximately independent of variations in nuclear capture rates but are functions of $\underline{a}$. In Fig. 9 predicted C^{12} pionic x-ray yields are shown as a function of $\Gamma_{2p}(\text{cap})$ for several values of $\underline{a}$. In this case, the relative yield L_β/L_α implied $\underline{a} = +0.49 \pm 0.09$ which was in turn used

in conjunction with the absolute yield of the K_α-line to obtain $\Gamma_{2p} = 2.6 \pm 0.9$ eV. This second technique was used for all elements except oxygen, magnesium, and titantium, for which insufficient yield data required use of the first technique. The results of this analysis are presented in Table VI. The level populations are listed for comparison with the results of other investigators who have done similar cascade calculations but have used different "initial" distributions. Best-fit calculated values have not been listed in Table V because generally the cascade parameters were not overdetermined.

Because $\Gamma_{n\ell}(\text{cap})$ is approximately proportional to $\Gamma_{n\ell}^{n'\ell'}(\text{rad})$ for the transitions investigated in the present work, systematic errors in the calculations of the radiative-transition rates are directly reflected in the deduced values for $\Gamma_{n\ell}(\text{cap})$. Exact pionic 2p-1s radiative rates which have been calculated[18] for Be^9, C^{12}, and O^{16} were used in the present analysis. These calculations incorporated not only the strong-interaction energy shift of the 1s state but also the distortion of the 1s and 2p-state wave functions. For the 2p-1s transition in Li^6 hydrogenic wave functions were used in conjunction with the experimental energy for this transition in order to obtain the radiative rate. From the results of Ref. 18, we estimated that the 3d-2p calculated radiative rates in Mg and Ti should be increased by 0.7% and 2%, respectively, to compensate for strong-interaction effects. It is assumed that the errors introduced by using these approximate rates for Li, Mg and Ti are much smaller than the assigned uncertainties in the values for the yields and the state populations.

The cascade calculation, constrained to reproduce the observed x-ray yields, predicts the population probability and the capture probability for all pionic states in the atom. The products of these two probabilities constitute the capture schedule for the mesic atom. The capture schedule for the lower levels in pionic Li^6 is given in Table VII.

D. Effects of Finite Electron-Refilling Times

In the cascade calculations just described it has been implicitly assumed that all electron bound states in the mesic atom are filled whenever the meson makes an electromagnetic transition. In fact, of course, to fill an electron vacancy (created by an Auger process) requires a finite time which depends on the quantum number of the vacancy, the ionization state of the atom, and the electronic properties of the host material.

Estimates of refilling times were obtained from experimental and theoretical values [73] of florescence yields ω_K and ω_L for K and L-shell electron vacancies, where the florescence yield is the probability that the vacancy will be filled <u>via</u> a radiative transition. The competing process is that of Auger emission in which two vacancies are produced in the higher shell from which the original vacancy was refilled. The K florescence yield is then the ratio of the rates:

$$\omega_K = \lambda_K(\text{radiative})/\lambda_K(\text{total})$$

where

$$\lambda_K(\text{total}) = \lambda_K(\text{radiative}) + \lambda_K(\text{Auger})$$

For an isolated oxygen atom it has been estimated[73] $\omega_K = 0.0045$. The electronic 2p→1s radiative rate is $\lambda_K(\text{rad}) \approx 3 \times 10^{12}$ sec^{-1} which implies a total refilling rate

$$\lambda_K(\text{total}) \approx 6 \times 10^{14} \text{ sec}^{-1} \tag{13}$$

For a reasonable number of L-shell electrons in the atom this result should be essentially independent of Z. The above estimate is in reasonable agreement with the results of a recent detailed calculation[74] for neon which predicts a K-shell refilling rate of 3.71×10^{14} sec^{-1}. Similarly, an examination of typical L-shell florescence yields indicates, for isolated atoms, an L-shell refilling rate

$$\lambda_L(\text{total}) \approx 3 \times 10^{15} \text{ sec}^{-1}. \tag{14}$$

For atoms embedded in solids or liquids, there will be significant corrections to these rates, especially for low-Z elements. For example, if the L-shell comprises the conduction band as it does in Li, Be, and C the refilling rate for "L-shell" vacancies will be dependent on the characteristics of the lattice.[75] In addition, the rate for refilling K-shell vacancies from the conduction band is expected to differ from that for refilling from the L-shell in an isolated atom, and estimates of the difference are subject to large uncertainties. In higher Z atoms the possibilities exist of high degrees of ionization, ionization of neighboring atoms, and displacement of the ion in the lattice.[76] In view of the many complicating factors, the estimates (13) and (14) were taken as initial guesses in our calculations and were varied by an order of magnitude in investigating the effects of finite refilling times.

In Table VIII are listed the total electromagnetic transition rates for muons in C^{12} calculated with the assumption that all five electron states are filled. Auger emission of K-shell electrons dominates for transitions from levels above the dashed line (emission of L-shell electrons becomes significant for $n > 11$). Comparing these transition rates with the refilling rate (13), it is seen that the atom should be partially ionized when the meson occupies states in the vicinity of and above the solid line in Table VIII. The radiative transition rates out of these states are so small that the meson remains in these states until the electron K-shell is at least partially refilled. Thus the Auger process still determines the nature of the cascade, and the populations of the lower levels will be unaffected. Arguments identical to these may be applied to the other elements under investigation.

If, however, the K-shell refilling rate is substantially smaller than (13), then radiative rates will begin to compete effectively with Auger rates in mesic states with $n \sim 4$. The character of the cascade will then change because of the preference for large changes in n by radiative transitions as opposed to the $\Delta n = 1$ transitions preferred by Auger processes.

There have been two approaches to the problems posed by finite electron-refilling times. Eisenberg and Kessler[12] emphasized that the nature of the cascade would be unaffected for high n where the Auger process dominates; in the lower levels where radiation begins to compete, total transition rates were assumed small enough to permit complete refilling. Therefore, they made no explicit adjustment in the calculation to reflect incomplete refilling of the electron states, and any

possible effects on the nature of the cascade were absorbed into an adjustable parameter used to describe the initial distribution.

Suzuki,[77] de Borde,[65] and Berezin et al.[16] simulated the effects of finite refilling times by assuming a small equilibrium electron population in the mesic atom which was maintained throughout the meson cascade. This was accomplished by reducing the calculated Auger rates to reflect the reduced occupation probability of the electron states. The assumption that the number of electron vacancies is independent of the initial meson state appears tenuous in view of the large differences in transition rates displayed in Table VIII.

In the present work it was assumed that the refilling of vacancies in the electronic K and L-shells could be characterized by average refilling times τ_K and τ_L which were treated as adjustable parameters. Beginning the cascade at n = 9 with an assumed initial population of the electron shells the calculation progresses through the cascade, computing the number of electron vacancies at the time the meson arrives at a given state, then refilling the vacancies to maximize the total transition rate out of that state. The total lifetime of the mesic level is obtained by combining in quadrature the refilling time and the inverse of the total Auger decay rate, then adding the result to the inverse of the total radiative decay rate. While this approach for calculating the effects of incomplete electron refilling is largely intuitive, the results of the calculations indicate that a more rigorous analysis is not warranted at this time.

The yields predicted by the cascade calculation for both muons and pions in all elements in the present study were affected less than 1% by refilling rates (13) and (14); the effects were less than 2%

when these rates were halved. In Mg and Ti refilling rates which were an order of magnitude smaller than (13) and (14) were found to alter the predicted yields by about 8%; however, the effect could be completely compensated for by an increase in $\underline{a}$, Eq. (12). These results contradict those of Ref. 77 in which it was found that the relative intensities of the muonic K-series in Mg could be described by a statistical initial distribution in ℓ if it were assumed that the refilling times were long enough to insure that the atom was always in a highly ionized state and, further, that the same intensities could not be obtained simply by increasing $\underline{a}$.

The Mg and Ti muonic x-ray yield data could not be reproduced by the present cascade calculation with an assumed initial distribution given in the form (12), even for very large refilling times. By trial and error an initial distribution was found which gave satisfactory results as listed in Table III. This special distribution is illustrated in Fig. 10 where it is compared with a statistical distribution and a modified statistical distribution Eq. (12) with $\underline{a} = +0.40$. It should be noted that this special form for the initial distribution, while not unique, does simulate the rather irregular cascade scheme recently predicted for large mesic molecules.[71]

VI. DISCUSSION

A. Summary of Experimental Results

The primary object of the present investigation was to determine the strong-interaction broadening of the 2p pionic levels in Li^6, Be^9, C^{12}, and O^{16}. The 2p widths in C^{12} and O^{16} are in clear disagreement with previously reported results, as can be seen from Table VI and Fig. 11. The primary source of the discrepancy is in the different values obtained for the absolute yields, as discussed in Sec. IV.D, and not in the level populations determined with the cascade calculations. The present results for Be^9, which are in excellent agreement with those of Backenstoss,[18] disagree with the published results of Berezin et al.,[16] again primarily because of different yield values. On the other hand, the apparent equality of the widths in Li^6 and Li^7 is due entirely to the different predictions for the 2p-level populations in the two elements. Because the level populations are largely determined by atomic properties, it is expected that the difference is computational rather than physical.

B. Comparison with Theory

The previously noted uncertainties and inconsistencies among the predictions (3), (4), and (5) of the field-theoretical calculations make comparison with experiment difficult. These theories generally have no adjustable parameters except for a variable which appears in the

phenomenological nucleon correlation function. In order to isolate the various effects which influence the absorption process and determine their relative importance, most authors omit other, often significant phenomena from their calculations. It is noteworthy that such calculations, in spite of these omissions, have predicted absolute absorption rates within a factor of five of the observed values. Furthermore, the dependence of the pion absorption rate on explicitly nuclear properties (e.g., nuclear excitations and final-state interactions) has been investigated, and the results should be useful for understanding discrepancies between the predictions of the phenomenological models and experimental observations.

The optical potential Eq. (8), which is based on a multiple-scattering theory, has, in principle, no adjustable parameters. However, because of the oversimplified form of the correlation function which was used in the derivation, the ad hoc correlation parameter ξ was introduced as a possible variable. Conforming with Krell and Ericson[21] we have set $\xi = 1$ in the present analysis. The model then predicts the absolute pion absorption rate, as well as the dependence of this rate upon Z and upon other properties of the nucleus. It should be realized, however, that the relative absorption rates for different nuclei are model-independent, to a first approximation. Thus agreement between theory and experiment upon the general Z (or A) dependence of the rates is no indication of the success of the present model. It is the ability of the theory to predict absolute rates and model-dependent phenomena, such as isospin effects, which must be examined.

By constraining the constant parameters in the optical potential such that the model "predicts" observed pionic x-ray energies and widths, one obtains a set of "best fit" parameters which may then be used to predict the energies and widths of x-ray lines which have not yet been measured. More significantly, the comparison of these parameters to those predicted from π-nucleon scattering lengths and pion production cross sections, as discussed in Sec. II., constitutes a test of hypotheses upon which these predictions are based. In particular the 2p, 3d, and 4f-level widths determine the "best fit" value for ImC_o in Eq. (8) while having relatively minor influence on the other parameters.[21] Isospin dependence of the absorption rates has been investigated and found to be negligible within the present experimental uncertainties.[43] Thus ImC_o is determined by essentially a one-parameter fit to the measured widths of the 2p, 3d, and 4f levels, for which there is a wealth of experimental data.[18]

The technique employed in the present analysis was to use optical-potential parameters obtained from a best fit to selected pionic x-ray data to predict 2p-level widths in low-Z elements.[78] The best-fit analysis was limited to direct linewidth measurements of monoisotopic, non-deformed nuclei whose charge distributions had been determined experimentally. The requirement that the linewidth be measured directly rather than by the indirect, yield method insured that the resulting best-fit parameters were not biased by possible systematic errors in the indirect method. Thirty-eight targets fulfilled the monoisotopic and spherical-nuclei requirements, and direct width measurements of either the 2p, 3d, or 4f level had been made in 16 of the 38 nuclei.

The optical potential of Anderson, Jenkins, and Powers[43] was used to analyse these data. It differs slightly from that of Eq. (8) in that the potential is written in a form emphasizing its dependence on the neutron, proton, and matter densities. Using the same notation as Eq. (8) and assuming spherical symmetry, they write:

$$q(r) = -4\pi[b_o'\rho(r)+b_1'(\rho_n(r)-\rho_p(r))+iImB_o'\rho(r)\rho_p(r)]$$

$$\alpha_0(r) = -4\pi[c_o'\rho(r)+c_1'(\rho_n(r)-\rho_p(r)+iImC_o'\rho(r)\rho_p(r)] \quad (15)$$

where

$$b_o' = p_1 b_o = 1.15 b_o$$

$$b_1' = p_1 b_1 = 1.15 b_1$$

$$B_o' = p_o B_o \rho(r)\rho_p(r) \approx 2.14 B_o$$

$$C_o' = p_1^{-1} C_o = 0.87 C_o \quad (16)$$

$$C_1' = p_1^{-1} C_1 = 0.87 C_1$$

$$C_o' = p_2^{-1} C_o \rho(r)/\rho_p(r) \approx 1.86 C_o$$

The methods used to determine the nucleon densities and the general calculational techniques are described in Ref. 43. The best-fit parameters (16) obtained from the selected pionic x-ray data are listed in Table IX. For comparison we list the parameters selected by Backenstoss[18] on the basis of a large set of x-ray data which was not restricted by any specific criteria and, in particular, included indirect width measurements. In column (3), Table IX are the theoretical

predictions taken from Ref. 21. We see that the agreement among the three sets of real parameters is quite good; both best-fit values for ImB_o are about a factor of two larger than the theoretical prediction; and the value for ImC_o obtained with the selected x-ray data is also a factor of two larger than predicted.

It is of interest to determine if the optical potential [Eqs. (8) and (15)] may be applied to low-Z elements without changing the constant parameters of column (2), Table IX. These best-fit parameters were, therefore, used to predict the 2p-level widths for elements with $A < 30$. These predictions are shown as a solid line in Fig. 11, where the open circles are the results of the present experiment, the open squares are from Ref. 16, and the open triangles from Ref. 18. The closed circles are the directly measured 2p linewidths of the selected nuclei used to obtain the best fit given by the solid curve for $A > 30$. The solid triangle is a revision[18] of an earlier direct measurement of the 2p-level width in P^{31}. This revision, because it represents such a small fraction of the total amount of data used, should have a very small effect on the best fit given by the solid curve.[79] The lower, broken line in Fig. 11 is the fit of Ref. 18 obtained with the potential Eq. (8) and the constant parameters of column (1), Table IX. It should be remembered that this lower curve was partially constrained by the widths indicated by the open triangles.

The advantage of displaying "reduced" widths (essentially division by Z^6) versus the atomic mass number A, as in Fig. 11, is that most of the model-independent behavior is removed. In the present case, because the isospin dependence of the width was assumed negligible, the

irregular shapes of the best-fit curves and the extrapolated curve are influenced by variations in the density factors $\rho_p(r)$, $\rho_n(r)$, and $\rho(r)$ among the different nuclei.

C. Conclusions

1. Experimental Techniques

Any comparison between the experimental technique used in the present investigation and that of the CERN group[19,20] will have to be tentative as only three points of comparison (Be^9, C^{12}, and O^{16}) are presently available. For C^{12} and O^{16} the discrepancy is irreconcilable although the uncertainties assigned to the present measurements are large. While the agreement between the two techniques for Be^9 is excellent, it should be noted that this width is clearly inconsistent with the trend indicated by the lower broken line of Fig. 11 and is in somewhat better agreement with predictions based on selected x-ray data (dashed line). The precision of the present technique would be improved through the use of thinner and smaller targets to reduce uncertainties in the self-absorption calculations and the geometrical corrections, higher-resolution detectors (unfortunately this usually implies smaller active volume) to reduce uncertainties in the background, and more data to reduce the statistical fluctuations. These improvements will necessitate longer data-accumulation times or more intense pion beams.

The CERN technique involves fewer corrections than the present method to obtain a yield value from the raw data and is, therefore, inherently capable of higher precision. Because the CERN method requires precise knowledge of the ratio of muons to pions stopping in

the target, it would seem worthwhile to check this ratio for several targets (e.g., C^{12} and O^{16}). This could be done by using the same technique to determine the absolute L-series yields as is used for the K-series yields. Because the L-series in these low-Z elements is relatively unaffected by nuclear absorption, their intensities may be determined with conventional cascade calculations constrained to reproduce the more precise relative yields (e.g., L_β/L_α).

2. The Optical Model

The results of the present experiment are in satisfactory agreement with predictions based on an optical-model potential whose constant parameters had been determined using selected data, largely from higher-Z elements. The best-fit parameters for the absorptive terms in this potential (ImB_o and ImC_o in column (2), Table IX) are in disagreement by factors of two with those predicted by the quasi-deuteron absorption model.

On the basis of the present experiment the possibility cannot be ruled out that the 2p absorption rates in low-Z elements are somewhat larger than those predicted by the optical model. If such a phenomenon exists, it would be interesting to determine if the same mechanism might not also be responsible for the apparent leveling-off of 1s absorption rates for $Z \geq 9$. More precise measurements of 2p-level widths are needed in the experimentally difficult range $12 < A < 40$.

The specifically nuclear effects of final-state interactions between the residual nucleus and the emitted nucleons and of nuclear

excitations are not considered in the quasi-deuteron absorption model. One might speculate that if these effects could be incorporated into the model, perhaps as corrections, a more realistic comparison with absolute rates should result. Until existing experimental and theoretical uncertainties are reduced, it seems unlikely that we will be able to obtain detailed nuclear structure information from pion absorption rates in complex nuclei.

3. Atomic Cascade Processes

The mixed Auger-radiative transition proposed by Ruderman[11] appears to be completely effective in depopulating the metastable muonic 2s level in elements with $Z < 6$ with the probable exception of Li. The results of the present experiment are not inconsistent with mixing rates calculated in Ref. 11; the calculated decay time for the 2s state via this transition is about 40 nsec for Li. Thus delayed-coincidence experiments are a possible means for investigating this phenomenon.

By using existing cascade calculations one may be able to investigate the possible formation of large mesomolecules[71] in elements for which several x-ray series are measured with good precision. The technique was suggested by the present analysis of muonic Mg and Ti for which the results could be interpreted in terms of the mesomolecule hypothesis.

VII. TABLES

Table I. Target properties and typical beam rates

Target	Covering	Target Thickness[a] (g/cm^2)	Lowest Energy X Ray Measured	Measured Absorption Coefficient at Lowest Energy (cm^{-1})	Target Thickness[c] (cm)
Li^6	Thin oil plus two layers Saran Wrap	1.95[b]	K_α-μ 18.6KeV	0.115±0.015[b]	2.54
Be^9	None	2.05	L_α-μ 6.1KeV	5.34±0.25	0.78
C^{12}	None	1.80	L_α-μ 13.9KeV	1.39±0.05	1.07
$(H_2)O^{16}$	Thin Mylar	2.46[d]	K_α-μ 134KeV	0.15±0.05[b]	1.75[d]
Mg	None	1.66	M_α-μ 19.5KeV	5.68±0.03	0.68
Ti	None	1.89	L_α-μ 191KeV	0.48±0.04	0.30

Typical Rates:[e]

Negatives into degrader	$700/cm^2$ sec
Pion Stops	$160/sec\ g/cm^2$
Muon Stops	$40/sec\ g/cm^2$

[a] Along beam axis

[b] Includes target covering

[c] Along target-detector axis

[d] Mean thickness

[e] Rates given are time-average for the stretched beam. The prompt beam was always gated out. Ratio of maximum rates to time-average rates was 3 to 5. For details refer to Beam CM-4, SREL Users Handbook, 1970 (unpublished).

Table II. Detectors

Detector	Dimensions (Nominal)	Bias	Resolution[a]	Window	Distance from Target center
Si(Li)	$80mm^2 x 3mm$	-250v	0.73KeV@26KeV	0.015cm Be	13.6cm
Ge(Li)	$350mm^2 x 5mm$	+500v	1.8KeV@74KeV	0.05cm Stainless Steel plus 0.05cm Al	12.3cm
Ge(Li)	$770mm^2 x 40mm$	+1000v	2.4KeV@74KeV	0.17cm Al	17.8cm

[a]Determined with mesic x-ray lines in pionic x ray spectra.

Table III. Summary of experimental muonic x-ray yields, and comparison with the results of the cascade calculations.

Element	Line	Energy (keV)	Yields Present	Yields Others	Calculated[a]
Li^6	K_α	18.6	0.67±0.08		0.67±0.03[d]
	K_β	22.1	0.22±0.03		0.22±0.02
	K_γ	23.3	0.03±0.01[b]		0.04±0.01[b]
	All K		0.92±0.12	0.83±0.03[c]	0.93±0.01[d]
				0.75±0.15[e]	
	K_α/All K		0.73±0.03	0.86±0.03[c]	0.72±0.03[d]
				0.72±0.05[e]	
Be^9	K_α	33.4	0.75±0.07		0.75±0.03[f]
	K_β	39.5	0.20±0.03		0.20±0.02
	K_γ	41.6	0.06±0.02[b]		0.05±0.02[b]
	All K		1.01±0.12	1.09±0.13[e]	1.00[f]
				1.01±0.10[g]	
	K_α/All K		0.74±0.03	0.83±0.07[e]	0.75±0.04[f]
				0.83±0.07[c]	
	L_α	6.1	0.48±0.15	0.33[e]	0.34±0.02
	L_β	8.4	0.021±0.015		0.025±0.002
	L_γ	9.3	0.003±0.002[b]		0.0025±0.0005[b]
	All L		0.50±0.17	0.38±0.09[e]	0.37±0.01
				0.32±0.03[h]	
	L_α/All L		0.95±0.03	0.78±0.04[c]	0.92±0.01

Table III. (continued)

Element	Line	Energy (keV)	Present	Yields Others	Calculated[a]
C^{12}	K_α	75.2	0.63±0.05		0.69±0.03[f]
	K_β	89.3	0.19±0.02		0.20±0.01
	K_γ	94.3	0.13±0.02[b]		0.10±0.02[b]
	All K		0.95±0.09	0.97±0.10[g]	1.00[f]
	K_α/All K		0.66±0.02	0.86±0.03[c]	0.69±0.03[f]
				0.71[g]	
	L_α	13.9	0.43±0.05		0.46±0.02
	L_β	18.9	0.08±0.03		0.070±0.004
	L_γ	21	0.02±0.01[b]		0.011±0.001
	All L		0.58±0.09	0.50±0.05[h]	0.54±0.02[b]
				0.50±0.10[e]	
	L_α/All L		0.81±0.04	0.80±0.03[c]	0.850±0.012
				0.83±0.07[e]	
O^{16}	K_α	134	0.59±0.05		0.608±0.022[f]
	K_β	158	0.17±0.02		0.181±0.004
	K_γ	167	0.14±0.02		0.140±0.010
	K_δ	170	0.085±0.015[b]		0.076±0.008[b]
	All K		0.98±0.10		1.00[f]
	K_α/All K		0.60±0.02	0.79±0.04[c]	0.608±0.022[f]
Mg	K_α	296		0.807±0.022[i]	0.780[f,j]
	K_β	353		0.068±0.007[i]	0.072
	K_γ	372		0.046±0.006[i]	0.048

Table III. (continued)

Element	Line	Energy (keV)	Present	Yields Others	Calculated[a]
Mg	K_δ	382		0.079±0.016[i,b]	0.100[b]
	L_α	56.4	0.55±0.05		0.607
	L_β	75.8	0.09±0.03		0.102
	L_γ	85	0.05±0.01		0.033
	L_δ	90	0.03±0.01[b]		0.019[b]
	All L		0.72±0.10	0.87±0.04[g]	0.761
	L_α/All L		0.76±0.03	0.75[g]	0.798
	M_α	19	0.42±0.07		0.347
	M_β	28	0.045±0.025		0.037
	M_γ	31	0.02±0.01[b]		0.011[b]
	All M		0.49±0.10		0.395
	M_α/All M		0.86±0.04		0.878
Ti	K_α	942		0.751±0.004[f,k]	0.751[f,j]
	K_β	1122		0.077±0.003[k]	0.070
	K_γ	1189		0.023±0.003[k]	0.023
	K_δ	1220		0.150±0.015[k]	0.156
	L_α	190.5	0.45±0.06		0.513
	L_β	257	0.05±0.01		0.115

Table III. Footnotes

---

[a]Best-fit for initial distribution Eq. (12). Corresponding values of a are listed in Table IV.

[b]Includes contributions from all higher-energy transitions in the series.

[c]M. B. Stearns et al. (1969), Ref. 15.

[d]Includes mixed-in contribution from 2s state; see text.

[e]S. Berezin et al. (1970), Ref. 16.

[f]Total K-series yield assumed equal to unity.

[g]J. L. Lathrop et al. (1961), Ref. 7.

[h]After M. B. Stearns et al. (1969), Ref. 15, with totak K-series yield equal to unity.

[i]After A. Suzuki (1967), Ref. 76. These values were used in determining the "initial" distribution, Table IV.

[j]Obtained using a special initial distribution, see text. Typical uncertainties are ± 10%.

[k]After D. Kessler et al., Phys. Rev. Letters 18, 1179 (1967). These values were used in determining the "initial" distribution, Table IV.

Table IV. Muonic-cascade parameters for a modified statistical distribution in initial level N = 9.

Element	a	Population
Li^6	+0.30±0.10	P_{2p}=0.67±0.03[a]
Be^9	+0.50±0.12	P_{2p}=0.75±0.03[a]
C^{12}	+0.32±0.07	P_{2p}=0.69±0.03[a]
O^{16}	+0.08±0.05	P_{2p}=0.61±0.03[a]
Mg	b	P_{3d}=0.60±0.05
Ti	b	P_{3d}=0.55±0.05

[a]Includes contribution from 2s state; see text.

[b]Special distribution used; see text.

Table V. Summary of experimental pionic x-ray yields.

Element	Line	Energy (keV)	Yield Present	Yield Others
Li^6	K_α	24.2	0.26±0.03	
	K_β	28.8	0.06±0.01	
	K_γ	30	0.018±0.005[a]	
	All K		0.34±0.05	
	K_α/All K		0.76±0.02	
Be^9	K_α	42.3	0.10±0.01	0.105±0.014[b]
				0.150±0.015[c]
	K_β	50	0.025±0.006	
	K_γ	53	0.013±0.004[a]	
	All K		0.14±0.02	0.21±0.05[d]
				0.188±0.017[c]
				0.21±0.02[e]
	K_α/All K		0.71±0.04	0.90±0.10[d]
				0.80[c]
				0.74[e]
	L_α	8.0	0.37±0.05	
	L_β	11	0.032±0.006	
	L_γ	12	0.003±0.001[a]	
	All L		0.41±0.06	0.35±0.07[d]
	L_α/All L		0.90±0.02	0.80±0.06[d]

Table V. (continued)

Element	Line	Energy (keV)	Yield Present	Yield Others
C^{12}	K_α	93.2	0.035±0.010	0.075±0.020[b]
				0.076±0.009[c]
				0.082±0.006[f]
	K_β	112	0.006±0.002	
	All K		0.045±0.014	0.095±0.010[c]
				0.15 +0.001 -0.02[e]
	K_α/All K		0.78	0.80[c]
				0.78[e]
	L_α	18.4	0.50±0.07	
	L_β	25	0.09±0.01	
	L_γ	27	0.010±0.005[a]	
	All L		0.60±0.08	0.36±0.10[d]
	L_α/All L		0.83±0.02	0.84±0.07[d]
O^{16}	K_α	160	0.020±0.005	0.049±0.007[g]
				0.031±0.010[c]
				0.034[e]
	K_β	194	≤0.003	
	All K		0.024±0.006	0.034±0.004[c]
				0.046±0.006[e]
	K_α/All K		0.83	0.91[c]
				0.74[e]

Table V. (continued)

Element	Line	Energy (keV)	Yield Present	Yield Others
Mg	L_α	74.3	0.49±0.05	
	L_β	101	0.066±0.007	
	L_γ	113	0.035±0.008[a]	
	All L		0.59±0.06	0.67±0.04[h]
				0.50±0.04[i]
	L_α/All L		0.84±0.02	0.84[h]
				0.79±0.10[i]
	M_α	25.9	0.46±0.04	
	M_β	38	0.040±0.008	
	M_γ	43	0.004±0.002[a]	
	All M		0.51±0.05	
	M_α/All M		0.91±0.02	
	N_α	12	0.17±0.04	
Ti	L_α	255	0.17±0.02	$0.16^{+0.17}_{-0.08}$[i]
				0.188±0.028[f]

[a] Includes contributions from all higher-energy transitions in the series.

[b] H. Koch et al. (1969), Ref. 20.

[c] M. Camac et al. (1955), Ref. 62.

[d] S. Berezin et al. (1970), Ref. 16.

[e] M. Stearns et al. (1957), Ref. 5.

[f] R. Kunselman (1969), Ref. 63.

[g] H. Koch et al. (1968), Ref. 19.

[h] M. B. Stearns et al. (1957), Ref. 6.

[i] M. Camac et al. (1955), Ref. 3.

Table VI. Pionic cascade parameters for a modified statistical distribution Eq. (12) in initial level N = 9.

Element	a	Population	Γ_{1s} (keV)	Γ_{2p} (eV)	Γ_{3d} (10^{-3}eV)
Li^6	+0.73±0.12	P_{2p}=0.68±0.04	0.15[a]	0.015±0.004	2×10^{-5} [a]
Li^7		P_{2p}≤0.40[b]		0.016±0.007[b]	
Be^9	+0.53±0.07	P_{2p}=0.64±0.03	0.58[a]	0.16±0.03	3×10^{-4} [a]
		≤0.55[b]		0.053±0.013[b]	
		=0.67±0.07[c]		0.16±0.03[c]	
C^{12}	+0.49±0.09	P_{2p}=0.67±0.04	3.25[a]	2.6±0.9	0.015[a]
		=0.62±0.06[c]		1.02±0.29[c]	
O^{16}	+0.14±0.06	P_{2p}=0.57±0.04	7.56[a]	12±4	0.220[a]
		=0.57±0.06[c]		4.7±0.8[c]	
Mg	d	P_{3d}=0.58±0.07	20[a]	100[a]	50±20
Ti	d	P_{3d}=0.50±0.06	300[a]	2890[a]	2700±900
					2500±700[c]

[a] Assumed known for the cascade calculations.

[b] D. P. Eartly, Thesis, University of Chicago, 1969 (unpublished) and Ref. 16.

[c] G. Backenstoss (1970), Ref. 18

[d] Special distribution used; see text.

Table VII. Nuclear capture schedule for pions in Li^6. Listed are the number of pions captured from each state per atomically captured pion.

n \ ℓ	0	1
5	0.006±0.004	0.0050±0.0005
4	0.016±0.006	0.035±0.001
3	0.022±0.007	0.130±0.006
2	0.019±0.005	0.430±0.075
1	0.335±0.065	

Total d-state capture:	$\sim 1 \times 10^{-5}$
Total p-state capture:	0.60±0.09
Total s-state capture:	0.40±0.09

Table VIII. Total electromagnetic decay rates for levels $n \leq 9$ in muonic C^{12} assuming all five electron states are filled. Units are 10^{14} sec^{-1}. Auger processes dominate above the dashed line. The atom is expected to be partially ionized above the solid line; see text.

n \ ℓ	0	1	2	3	4	5	6	7	8
9	2.50	2.79	3.35	4.26	5.56	7.30	9.56	12.4	15.9
8	1.77	2.04	2.53	3.33	4.47	5.98	7.92	10.3	
7	1.06	1.29	1.67	2.31	3.23	4.46	6.03		
6	0.52	0.72	0.97	1.44	2.12	3.04			
5	0.20	0.39	0.51	0.80	1.25				
4	0.06	0.31	0.26	0.39					
3	0.02	0.52	0.23						
2	a	1.66							

[a] The 2s↔2p→1s transition is expected to depopulate the 2s state at a rate greatly exceeding the 2s→1s Auger rate. See discussion, Section IV.C.

Table IX. Parameters of the nuclear optical potential, where μ is the pion rest mass.

Parameter	From experiment, Backenstoss[a] (1)	From experiment, after Anderson et al.[b] (2)	Theory[c] (3)
$b_0[\mu^{-1}]$	-0.030	-0.029 ± 0.001	-0.023
$b_1[\mu^{-1}]$	-0.08	-0.102 ± 0.017	-0.09
$c_0[\mu^{-3}]$	+0.22	$+0.23\pm0.01$	+0.19
$c_1[\mu^{-3}]$	+0.18	$+0.16\pm0.13$	+0.18
$\mathrm{Im}B_0[\mu^{-4}]$	+0.040	$+0.036\pm0.002$	+0.017
$\mathrm{Im}C_0[\mu^{-6}]$	+0.08	$+0.161\pm0.019$	+0.073

[a] Ref. 18.

[b] Ref. 43. Eqs. (16) have been used to compare the parameters of Table I, Ref. 43, with those of columns (1) and (3) above.

[c] Krell and Ericson, Ref. 21.

VIII. ACKNOWLEDGMENTS

The author would like to acknowledge the following persons for their contribution and support.

Dr. Robert E. Welsh, his advisor, who has provided valuable criticism and encouragement during all phases of this research and in the preparation of the manuscript.

Dr. Robert T. Siegel, who suggested this experiment, for his guidance and helpful discussions.

Dr. Morton Eckhause for invaluable assistance in the experimental runs and careful reading of the manuscript.

Dr. David K. Anderson for helpful and stimulating discussions concerning the theoretical aspects of this work and for the generous contribution of his time and effort in computing the predicted level widths.

Drs. Rolf G. Winter and Richard J. Powers for helpful discussions and reading the manuscript.

Dr. David A. Jenkins for useful discussions and reading the manuscript and for bringing to his attention the refilling calculations of H. P. Kelly, et al.

Dr. Herbert Friedman for reading the manuscript.

Drs. Gideon Weisz and Arden Sher for helpful discussions.

Dr. Jörg Hüfner for providing an annotated copy of his muon cascade program.

Drs. John R. Kane and W. J. Kossler for interesting discussions on the meson capture and cascade processes.

Dr. William B. Shuler for his aid in taking the data.

Mr. George H. Miller for his invaluable assistance with the solid-state detectors and for his aid tendered during the experimental runs.

Mr. Darrell G. Eisenhut for his help in analysing the x-ray spectra.

Mrs. Gail S. Hunt for her aid in adapting and modifying the cascade program.

Mr. Donald S. Makowiecki and Mr. Erwin Bointin for their aid in maintaining the electronics.

Mr. Stanley G. Hummel and the Physics Department machine shop for construction of the scintillation counters, the target positioning brackets, and much of the cryogenic equipment.

The staff of the Space Radiation Effects Laboratory for their efficient and reliable operation of the synchrocyclotron.

The staff of the William and Mary Computer Center for their help and support during the programming and data analysis.

His fellow graduate students, particularly Miss Betty D. Orrick and Mr. C. William Lucas, for interesting discussions on many aspects of this investigation.

Mrs. Sylvia J. Stout and Miss Dianne D. Britton for typing the manuscript and the tables.

The J. E. Zollinger Fellowship Fund which supported the author during a portion of this work.

This work was supported in part by the National Aeronautics and Space Administration and the National Science Foundation.

IX. FOOTNOTES AND REFERENCES

1. Three comprehensive reviews of mesic atoms have been recently published: E.H.S. Burhop, High Energy Physics (Academic Press, Inc., New York, 1969), Vol. 3, pp. 109-281; S. Devons and I. Duerdoth, Advances in Nuclear Physics (Plenum Press, Inc., New York, 1969), Vol. 2, pp. 294-423; C.S. Wu and L. Wilets, Ann. Rev. Nucl. Sci. 19, 527 (1969). These reviews give references to theoretical and experimental investigations published since the review by D. West, Ref. 9, and up through early 1968. Reviews by F. Scheck, Ref. 61, and H. Daniel, Mesic Atoms (Technische Hochschule, Munchen, 1969) unpublished, contain references to work published after 1968.
2. The anomaly in low Z elements suggested by the results of M. Camac et al.,Ref. 3,was not fully recognized until the work by M.B. Stearns and M. Stearns, Ref. 4.
3. M. Camac, M.L. Halbert, and J.B. Platt, Phys. Rev. 99, 905 (1955).
4. M.B. Stearns and M. Stearns, Phys. Rev. 105, 1573 (1957).
5. M. Stearns and M.B. Stearns, Phys. Rev. 107, 1709 (1957).
6. M.B. Stearns, M. Stearns, and L. Leipuner, Phys. Rev. 108, 445 (1957).
7. J.L. Lathrop, R.A. Lundy, V. Telegdi, and R. Winston, Phys. Rev. Letters 7, 147 (1961).
8. A. Pevsner, R. Strand, L. Madansky, and T. Toohig, Nuovo Cimento 19, 409 (1961).

9. D. West, Repts. Progr. Phys. 21, 271 (1958).

10. T.B. Day and P. Morrison, Phys. Rev. 107, 912 (1957); J.B. Bernstein and Ta-Yon Wu, Phys. Rev. Letters 2, 404 (1959); N.A. Krall and E. Gerjuoy, Phys. Rev. Letters 3, 142 (1959); R.A. Ferrell, Phys. Rev. Letters 4, 425 (1960).

11. M.A. Ruderman, Phys. Rev. 118, 1632 (1960).

12. Y. Eisenberg and D. Kessler, Nuovo Cimento 19, 1195 (1961).

13. Y. Eisenberg and D. Kessler, Phys. Rev. 123, 1472 (1961).

14. Y. Eisenberg and D. Kessler, Phys. Rev. 130, 2349 (1963).

15. M. Stearns, M.B. Stearns, G. Culligan, B. Sherwood, and V.L. Telegdi, Bull. Am. Phys. Soc. 9, 81 (1964); M.B. Stearns, G. Culligan, B. Sherwood, and V.L. Telegdi, Phys. Rev. 184, 22 (1969).

16. S. Berezin, G. Burleson, D. Eartly, A. Roberts, and T.O. White, Nucl. Phys. B16, 389 (1970).

17. Direct measurement of the width of spectral lines obtained using high-resolution detectors indicate that Γ can be measured to a precision of 30 eV under very favorable circumstances [R.J. Wetmore, D.C. Buckle, J.R. Kane, and R.T. Siegel, Phys. Rev. Letters 19, 1003 (1967) and R.J. Harris, Jr. et al, Ref. 50.] The yield method has been used to measure Γ(cap) over a range of 0.02 eV to 35 eV with precisions of .01 eV to 8 eV respectively (Ref. 18), although there may be undisclosed systematic errors.

18. G. Backenstoss, Proceedings of the Third International Conference on High Energy Physics and Nuclear Structure, edited by S. Devons (Plenum Publishing Co., New York, 1970) p. 469.

19. H. Koch, G. Poelz, H. Schmitt, L. Tauscher, G. Backenstoss, S. Charalambus, and H. Daniel, Phys. Letters 28B, 280 (1968).

20. H. Koch, M. Krell, Ch.v.d. Malsburg, G. Poelz, H. Schmitt, L. Tauscher, G. Backenstoss, S. Charalambus, and H. Daniel, Phys. Letters 29B, 140 (1969).

21. M. Krell and T.E.O. Ericson, Nucl. Phys. B11, 521 (1969).

22. Radiative π-capture in Li^6 is investigated by J. Delorme, Nucl. Phys. B19, 573 (1970) and P. Pascual and A. Fujii, Nuovo Cimento 65, 411 (1970); both papers contain references to earlier work. Calculations using assumed capture schedules for Li^6 have been reported by G. Alberi and L. Taffara, Nuovo Cimento 58, 441 (1968); D. Koltun and A. Reitan, Ref. 23; and Y. Sakamoto, Nucl. Phys. 87, 414 (1966).

23. D. Koltun and A. Reitan, Phys. Rev. 155, 1139 (1967).

24. J. Le Tourneux, Nucl. Phys. 81, 401 (1966).

25. D.H. Perkins, Phil. Mag. 40, 601 (1949).

26. K.A. Brueckner, R. Serber, and K.M. Watson, Phys. Rev. 84, 258 (1951).

27. J.L. Gammel and R.M. Thaler, Phys. Rev. 107, 291 (1957).

28. M. Ericson, Compt. Rend. 258, 1471 (1964).

29. G. Backenstoss, Ref. 18, gives references to earlier work. See also D.K. Anderson, D.A. Jenkins, and R.J. Powers, Phys. Rev. 188, 9 (1969).

30. M.E. Nordberg, Jr., K.F. Kinsey, and R.L. Burman, Phys. Rev. 165, 1096 (1968), contains references to earlier work.

31. R. S. Kaushal and Y. R. Waghmare, Nucl. Phys. A144, 449 (1970), contains a summary of earlier work.

32. For a complete discussion of the form of the π-nuclear interaction, see for example J. D. Jackson, The Physics of Elementary Particles (Princeton University Press, Princeton, N. J., 1958) p.4 ff and S. De Benedetti, Nuclear Interactions (John Wiley & Sons, Inc., New York, 1964) p. 434 ff.

33. M. V. Barnhill, III, Nucl. Phys. A131, 106 (1969).

34. Il-T. Cheon, Suppl. Prog. Theor. Phys., Extra Number, 146 (1968).

35. Il-T. Cheon, Phys. Rev. 158, 900 (1967).

36. K. Chung, M. Danos, and M. G. Huber, Phys. Letters 29B, 265 (1969).

37. W. Elsaesser and J. M. Eisenberg, Nucl. Phys. A144, 441 (1970).

38. R. M. Spector, Phys. Rev. B101, 134 (1964) and Kaushall and Waghmare, Ref. 8, find it possible to ignore initial-state correlations in particular formalisms. See also G. E. Brown, Comments Nuclear Particle Phys. 3, 78 (1969).

39. H. W. Bertini, Phys. Letters 30B, 300 (1969); H. J. Weber, Phys. Rev. Letters 23, 178 (1969).

40. D. S. Koltun and A. Reitan, Ref. 23; D. S. Koltun and A. Reitan, Phys. Rev. 141, 1413 (1966); and Il-T. Cheon, Nucl. Phys. A121, 679 (1968).

41. M. Ericson and T. E. O. Ericson, Ann. Phys. (N.Y.) 36, 323 (1966).

42. This form for the optical potential is that used in Ref. 21. In a recent analysis D. K. Anderson et al., Ref. 43, introduced two-nucleon isospin corrections which were subsequently found to be consistent with zero.

43. D.K. Anderson, D.A. Jenkins, and R.J. Powers, Phys. Rev. Letters 24, 71 (1970).

44. E. Storm and H.I. Israel, LA-3753, Los Alamos Scientific Laboratory, (1967).

45. The techniques and application of solid-state detectors in x-ray spectrometers have been extensively reviewed. See, for example, A.J. Tavendale, Ann. Rev. Nuclear Science 17, 73 (1967) and D.W. Aitken, IEEE Trans. Nuclear Science NS-15,10 (1968). The front-end configuration used in this experiment was identical to that described by R.J. Harris, Jr. and W.B. Shuler, Nucl. Instr. and Meth. 51, 341 (1967). See also R.J. Harris, Jr., Ref. 46, and W.B. Shuler, Ref. 47.

46. R.J. Harris, Jr., College of William and Mary Report WM-12, 1969 (unpublished).

47. W.B. Shuler, College of William and Mary Report WM-13, 1969 (unpublished).

48. Suggested by D. Jenkins, private communication; for detailed description see Refs. 46, 47.

49. Single Solid Gamma Sources, International Atomic Energy Agency, Vienna, Austria.

50. R.J. Harris, Jr., W.B. Shuler, M. Eckhause, R.T. Siegel, and R.E. Welsh, Phys. Rev. Letters 20, 505 (1968).

51. G. Backenstoss, S. Charalambus, H. Daniel, H. Koch, G. Poelz, H. Schmitt, and L. Tauscher, Phys. Letters 25B, 547 (1967).

52. The computation procedure is described by R. J. Harris, Jr., Ref.46.

53. Unlike the Li and Be targets the Mg target is essentially opaque to these x rays whose energies are < 25 keV.

54. Reference 49; the single exception was the absolute intensity of the atomic K x-ray series in Fe^{57} following decay of Co^{57}. This was deduced to be 0.55 $\pm$ 0.02 x rays per disintegration from data obtained by W. Rubinson and K. P. Gopinathan, Phys. Rev. 170, 969 (1968) and by D. C. Hall and R. G. Albridge, Nucl. Phys. A91, 495 (1967).

55. D. P. Donnelly, J. J. Reidy, and M. L. Weidenbeck, Phys. Rev. 173, 1192 (1968).

56. L. B. Magnuson, Phys. Rev. 107, 161 (1957).

57. T. Yamazaki and J. M. Hollander, Nucl. Phys. 84, 505 (1966). See particularly their Fig. 3 (p. 510) showing relative photopeak efficiencies.

58. This latter feature justified the use of an efficiency calibration obtained with a different target in the few cases when that obtained with the target under investigation was confused by a coincident mesic x-ray peak.

59. The most convincing spectrum for this purpose was that of the muonic M-series in Mg. The absence of the pionic M_α x-ray peak enabled us to conclude that the pion contamination in the muon beam must have been less than 0.5%.

60. Isotropy has been questioned by the author and independently by W. J. Kossler (private communication) and F. Scheck, Ref. 61, who suggest that some memory of the original beam direction might be retained during the slowing-down and capture processes. If this occurs, m = 0 substates (initial beam direction is the reference axis) will be preferentially populated with the result that a

fraction of the x rays will have a probability for emission proportional to sin θ, where θ is measured with respect to the beam axis. In the present experiment with an angle between the target-detector axis and the beam axis of 45°, maximum anisotropy (implying a multiple-scattering angle of 0°) would have resulted in a 9% underestimate of the absolute yields. From an examination of the muonic K-series yields, it was estimated that the present experimental results are insensitive to anisotropies as large as ~ 0.5. The author is grateful to W. J. Kossler for helpful conversations on this topic.

61. F. Scheck, Lectures at the "SIN-Sommerschule fur Mittelenergie Physik" (Leysin, September, 1969) REF. TH. 1092-CERN (unpublished).

62. M. Camac, A. D. McGuire, J. B. Platt, and H. J. Schulte, Phys. Rev. 99, 897 (1955).

63. A. R. Kunselman, University of California (Berkeley) Report UCRL-18654, 1969 (unpublished).

64. We are greatly indebted to J. Hüfner who kindly provided us with a copy of his muon-cascade program.

65. A. H. de Borde, Proc. Phys. Soc. (London) A67, 57 (1954).

66. G. R. Burbidge and A. H. de Borde, Phys. Rev. 89, 189 (1953).

67. J. C. Slater, Quantum Theory of Atomic Structure, Vol. I (McGraw-Hill Book Company, Inc., New York, 1960) p. 227, ff.

68. More exact calculations using hydrogenic wave functions for the meson states give results for Z_{eff} (potential) which differ by less than 6% from the present values for muons in C^{12} (Fig. 7). I am grateful to D. K. Anderson for sending me a copy of his computer program which performs these calculations.

69. J. C. Slater, op. cit., p. 368 ff.

70. In the calculation of these ratios, the use of hydrogenic wave functions for states significantly distorted by the strong interaction introduces negligible error in the results of the cascade calculation. Nuclear absorption from these states so overwhelms the electromagnetic decay rates that the essentially 100% absorption probability is insensitive to scaling errors.

71. S. S. Gershtein, V. I. Petrukhin, L. I. Ponomarev, and Yu. D. Prokoshkin, Usp. Fiz. Nauk 97, 3 (1969) [translation: Sov. Phys. - Usp. 97, 1 (1969)].

72. L. Tausher, G. Backenstoss, S. Charalambus, H. Daniel, H. Koch, G. Poelz, and H. Schmitt, Phys. Letters 27A, 581 (1968).

73. E. H. S. Burhop, The Auger Effect (Cambridge University Press, N. Y., 1952).

74. Private communication from H. P. Kelly of calculations by R. L. Chase, H. P. Kelly, and H. S. Kohler, to be published.

75. The time that it takes the conduction electrons to "refill" a vacancy in the band may be roughly estimated in the following manner. The electrons on atoms which are nearest-neighbors to the vacancy will experience a force $F = e^2/r^2$ where e is the electron (hole) charge and $r = d/2$ for electrons near the periphery of the nearest-neighbors; d is the lattice spacing. In a cubic lattice, for example, there are six nearest-neighbors each with N free electrons. Then each free electron contributes a charge $e/6N$ to the vacancy, or, conversely, moves a distance $\sim d/6N$ before the vacancy is "refilled". The time required to do this is

$$t = \left(2 \frac{d}{6N} \frac{m}{F}\right)^{+\frac{1}{2}} = \left(\frac{12Ne^2}{md^3}\right)^{-\frac{1}{2}}$$

where m is the electron mass. We note that t is approximately equal to the reciprocal of the plasma frequency

$$\omega_p = \left(\frac{4\pi Ne^2}{md^3}\right)^{\frac{1}{2}}$$

which is of the order of 10^{16} sec^{-1} for these materials.

76. G. T. Condo, R. D. Hill, and A. D. Martin, Phys. Rev. 133, A1280 (1964).

77. A. Suzuki, Phys. Rev. Letters 19, 1005 (1967).

78. The author is grateful to D. K. Anderson, D. A. Jenkins, and R. J. Powers for the calculated predictions and for their permission to present these results.

79. D. K. Anderson, private communication.

X. FIGURES

Figure Captions

1. Counter geometry, target and detector positions in the experiment. The degrader upstream of counter 1 was used only during the muonic x-ray runs.
2. Block diagram of the electronics. The cyclotron-RF trigger pulse provided a timing reference for gating the equipment off during the prompt (unstretched) part of the beam spill. DGG = Delay Gate Generator; D = Discriminator; FA = Fast Amplifier; C = Coincidence unit; S = Scaler; LG = Logic Gate (and amplifier); LSD = Logic Shaper and Delay; DDLA = Double-Delay-Line Amplifier; SCTA = Single-Channel Timing Analyser; TAC = Time-to-Amplitude Converter; PHA = Pulse-Height Analyser.
3. Differential range curve obtained using a 3.6 g/cm^2 C^{12} target.
4. Timing spectrum for pionic x rays from Be^9. The energy range spanned was $\sim$ 8 keV to $\sim$ 50 keV. Timing information for the "good" events is stored in the upper 200 channels of the 400-channel analyser.
5. (a) Be^9 pionic x-ray spectrum. The combined counts in eight adjacent channels have been plotted. (b) C^{12} pionic x-ray spectrum. (c) O^{16} pionic x-ray spectrum. In (b) and (c) the combined counts in four adjacent channels have been plotted. Additional evidence for the contaminant peaks from aluminum and oxygen were obtained from other spectra.

6. Net absolute detector efficiencies *versus* energy. ●, obtained using calibrated sources, Ref. 54. Δ, relative values obtained using an uncalibrated Ba^{133} source. □, relative values calculated from known detector characteristics. The source-detector distances were 13.6 cm, 12.3 cm, and 15.3 cm for the Si(Li), planar Ge(Li), and coaxial Ge(Li) respectively.

7. Plots of effective charges experienced by the muon and the K-shell electrons when the muon is in state (n, $\ell = n - 1$) in C^{12}. It is assumed that all available electron states are filled. The "field" values are used to calculate wave functions; the "potential" values are used to calculate transition energies.

8. Predicted x-ray yields *versus* a for muons in C^{12}. A modified statistical distribution Eq. (12) was used for the initial population in $N = 9$, and electron-refilling times have been assumed short compared to typical muon transition times. A weighted average of a_1, a_2, a_3, and a_4 is taken as the a for the cascade.

9. Predicted pionic x-ray yields in C^{12} *versus* Γ_{2p} (cap) and for three values of a. $a = +0.49 \pm 0.09$ was determined by the L_β/L_α ratio; the experimental L_α yield is clearly consistent with this choice.

10. Population probability $P_{N\ell}$ *versus* ℓ in initial level $N = 9$; ●, distribution which best duplicates experimental yields in muonic Mg. For comparison we show Δ, a statistical distribution, and ✕, a modified statistical distribution Eq. (12) with $a = +0.40$.

11. Reduced 2p-level widths *versus* atomic number A. The two curves are based on semiphenomenological optical potentials for the pion-nucleus interaction with parameters obtained by fitting pionic x-ray data. The solid line results from the best fit to selected data (see text)

which included only directly measured line widths (e.g., 3d-2p line widths for targets with A > 30); this curve corresponds to the potential of Eqs. (8) and (15) with the constant parameters of column (2), Table IX. The broken line arises from the fit by Backenstoss to x-ray data which included the CERN indirect width measurements (Δ) and the recently revised, directly measured 2p width for P^{31} (▲); see Ref. 18. The other experimental points are as follows: ●, directly measured linewidths for selected nuclei (see text); ■, indirect measurements of Berezin et al. (Ref. 16); and ○, results of the present work.

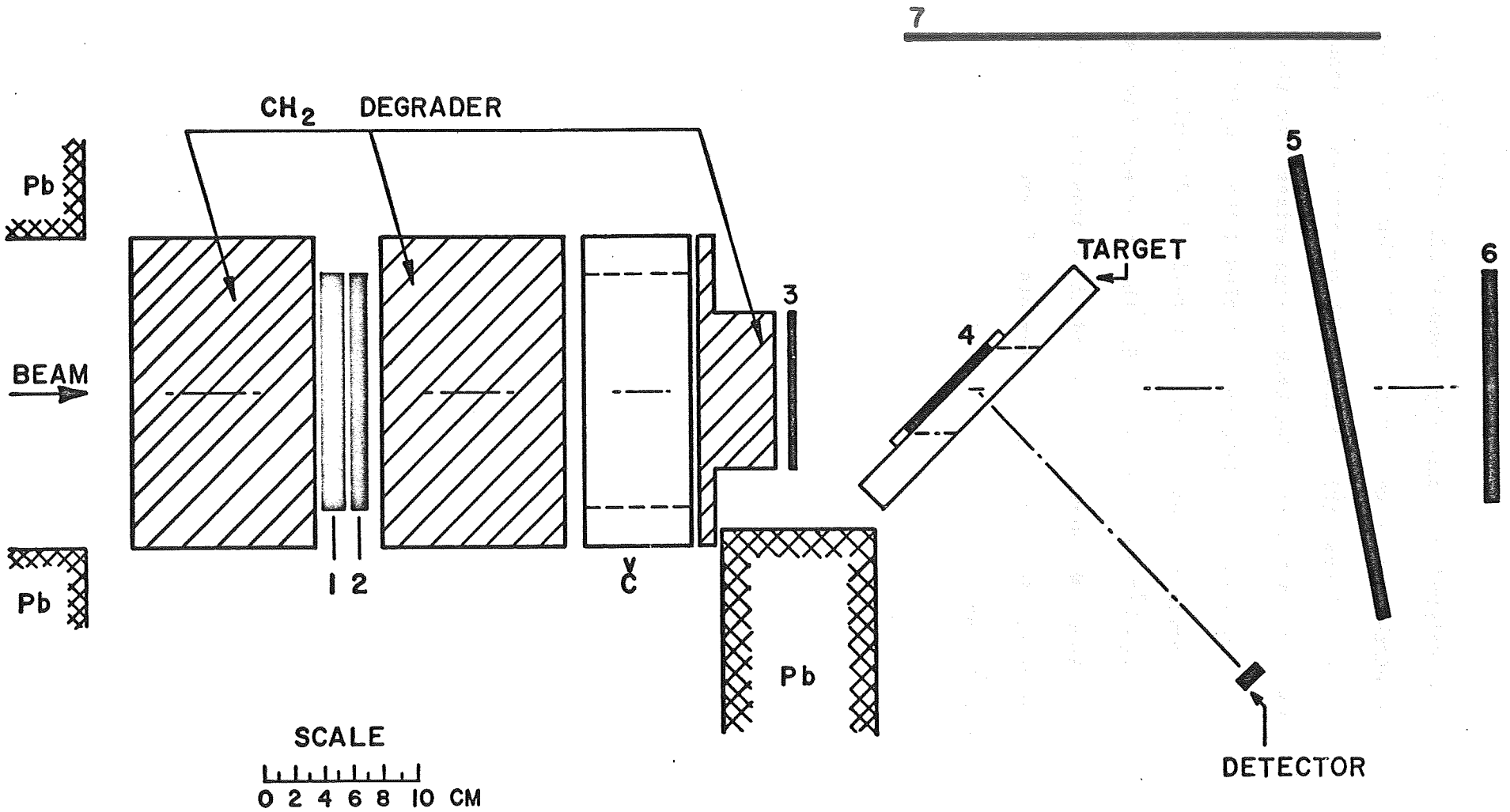
7
CH_2 DEGRADER
Pb
BEAM
Pb
1 2
C
3
4
TARGET
5
6
Pb
DETECTOR
SCALE
0 2 4 6 8 10 CM

FIG. 1

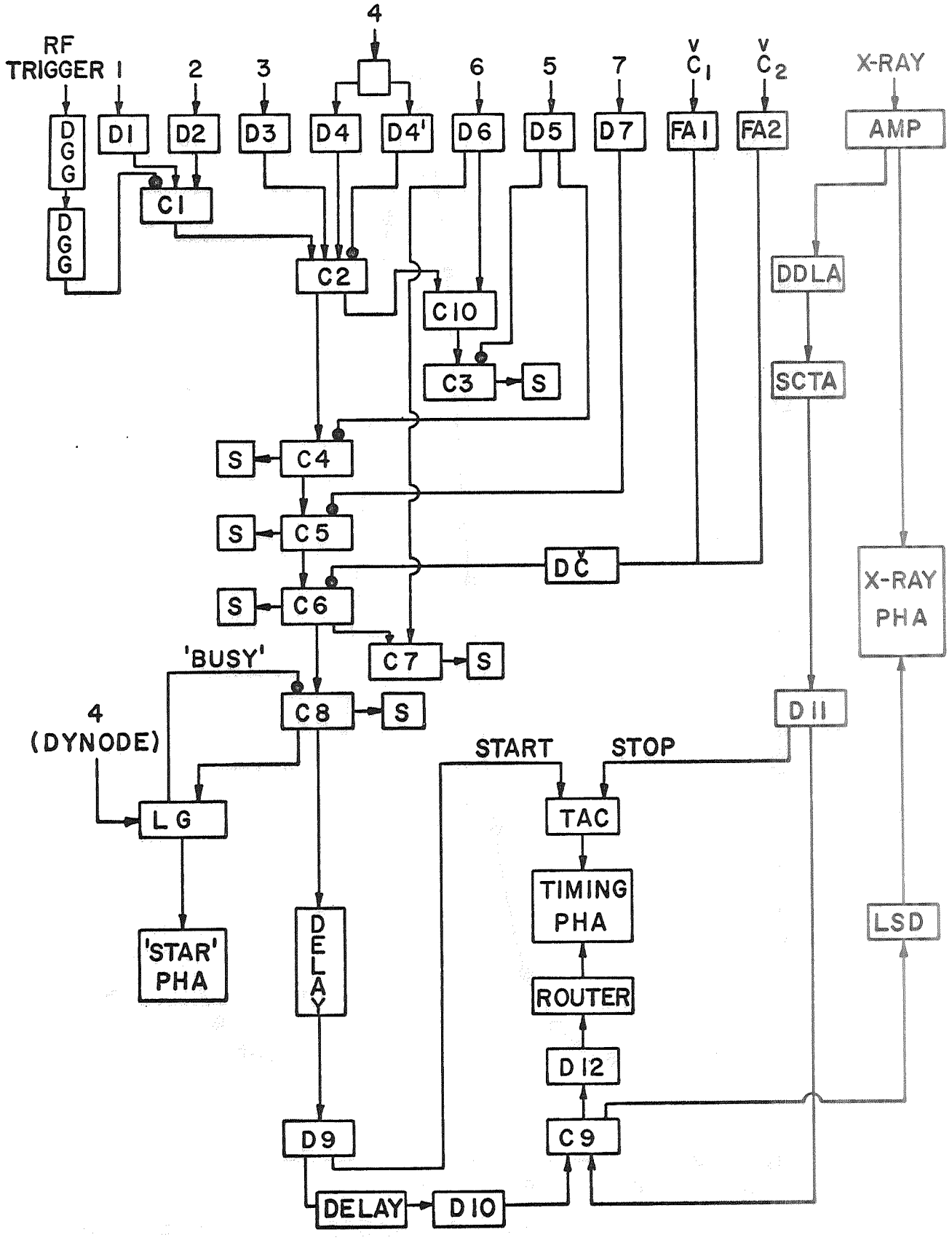
RF
TRIGGER
1
2
3
4
6
5
7
V C1
V C2
X-RAY
DGG
DGG
D1
D2
D3
D4
D4'
D6
D5
D7
FA1
FA2
AMP
C1
C2
C10
C3
S
DDLA
SCTA
S
C4
S
C5
DC
X-RAY PHA
S
C6
'BUSY'
C7
S
4
(DYNODE)
C8
S
D11
START
STOP
LG
TAC
TIMING PHA
'STAR' PHA
DELAY
ROUTER
LSD
D12
D9
C9
DELAY
D10

FIG. 2

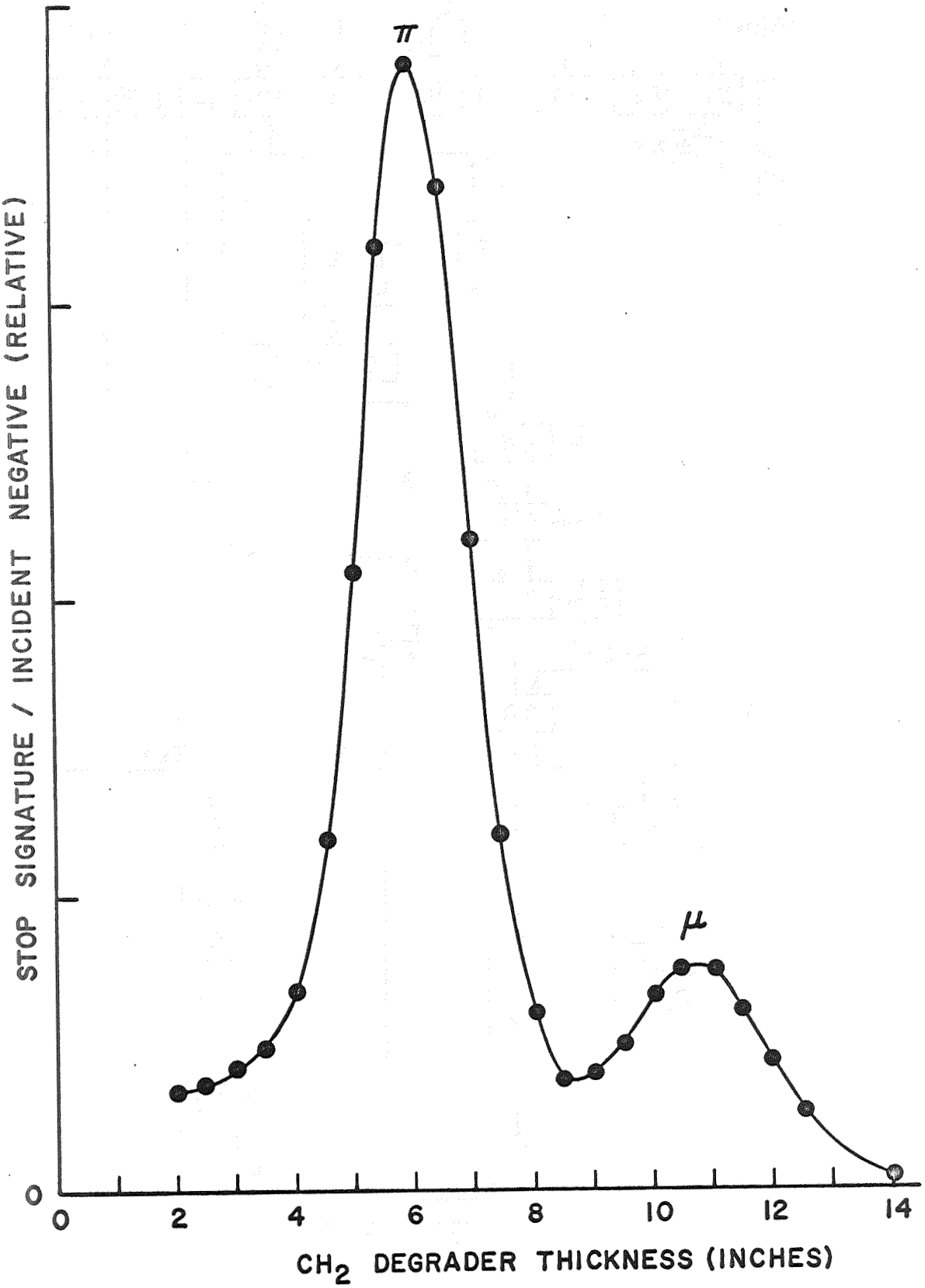
π
μ
STOP SIGNATURE / INCIDENT NEGATIVE (RELATIVE)
0
0
2
4
6
8
10
12
14
CH2 DEGRADER THICKNESS (INCHES)

FIG. 3

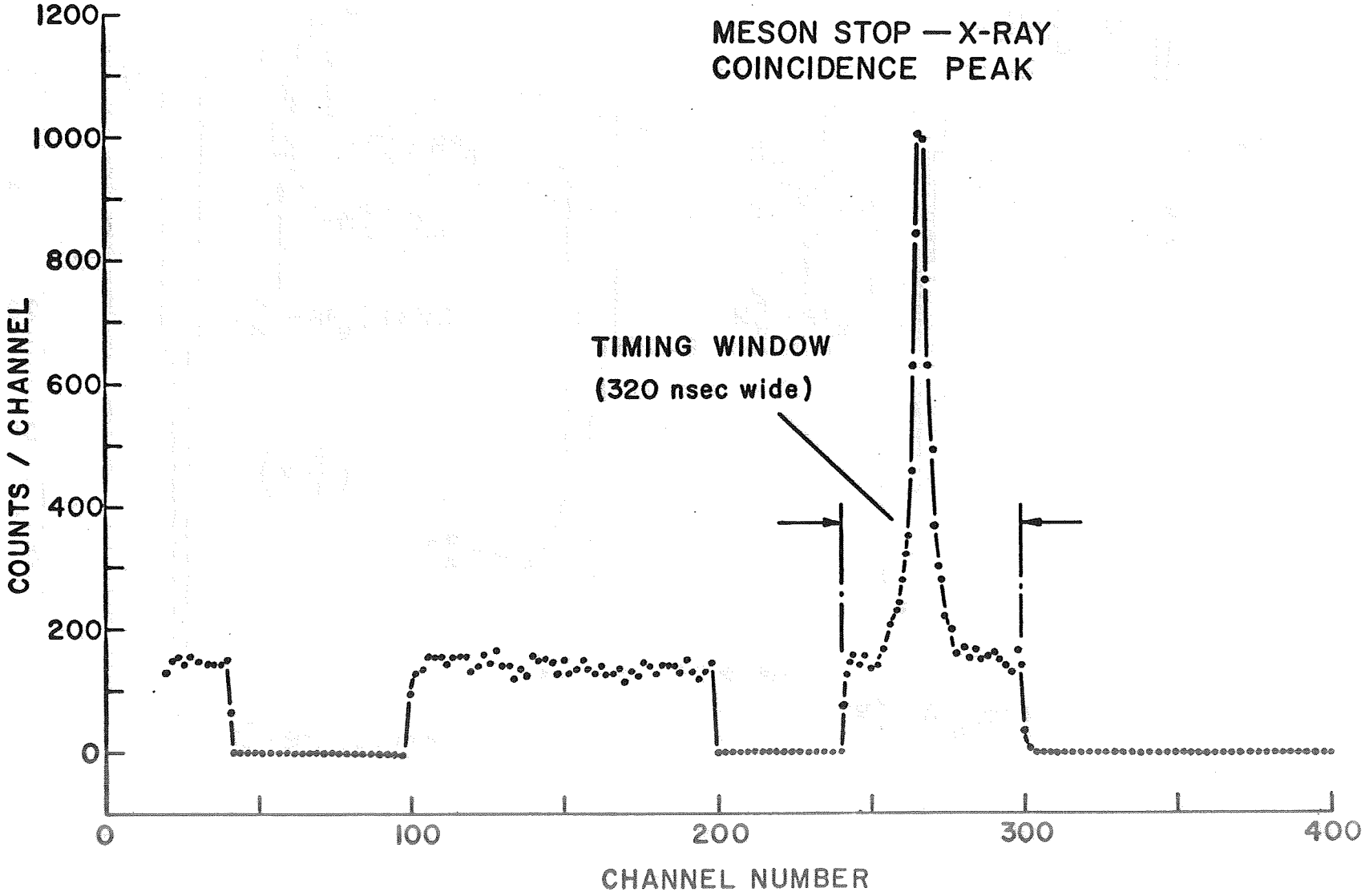
MESON STOP — X-RAY
COINCIDENCE PEAK
TIMING WINDOW
(320 nsec wide)
COUNTS / CHANNEL
1200
1000
800
600
400
200
0
0
100
200
300
400
CHANNEL NUMBER

FIG. 4

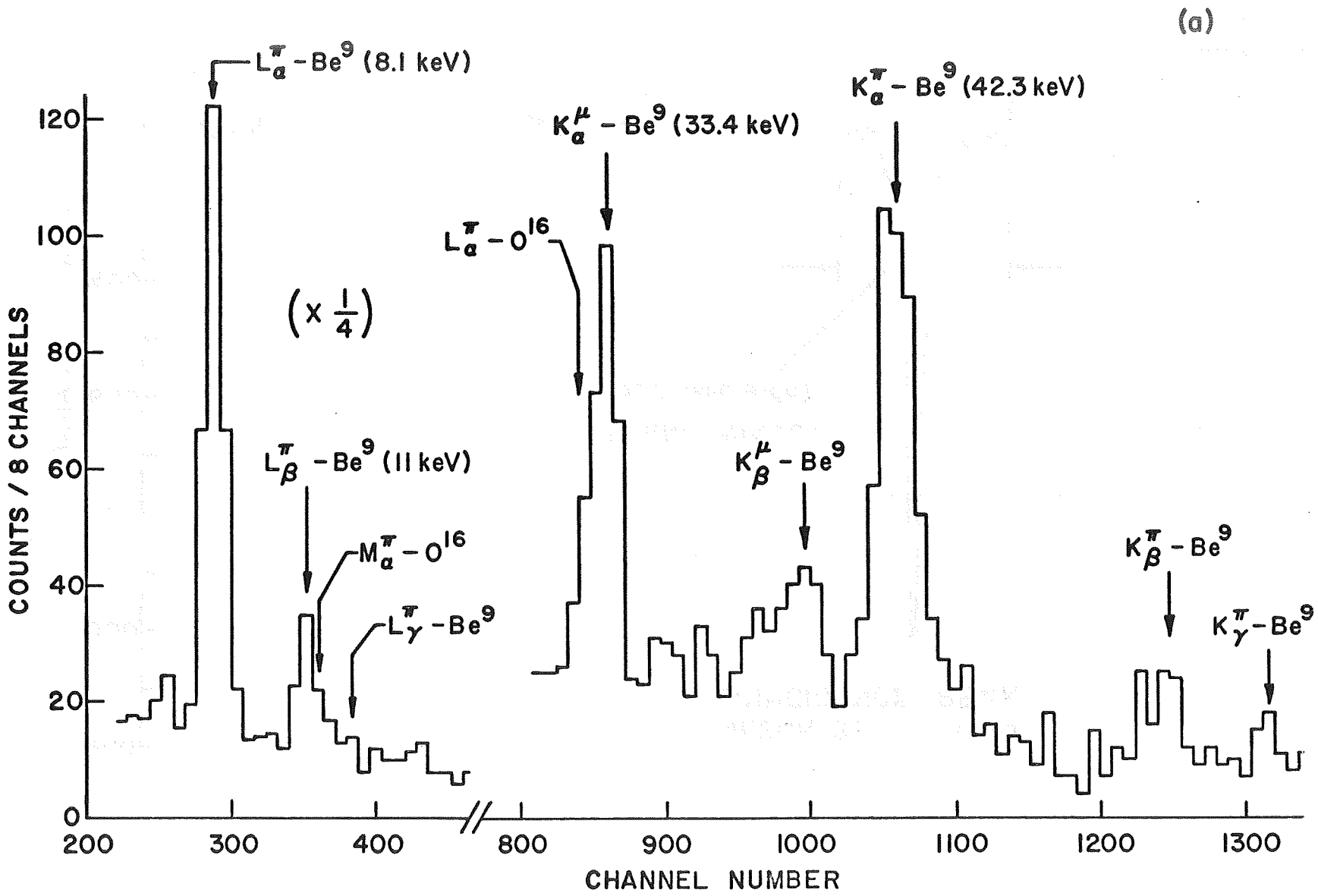
(a)
L_α^π - Be^9 (8.1 keV)
K_α^μ - Be^9 (33.4 keV)
K_α^π - Be^9 (42.3 keV)
L_α^π - O^{16}
(× 1/4)
L_β^π - Be^9 (11 keV)
M_α^π - O^{16}
L_γ^π - Be^9
K_β^μ - Be^9
K_β^π - Be^9
K_γ^π - Be^9
COUNTS / 8 CHANNELS
0
20
40
60
80
100
120
200
300
400
800
900
1000
1100
1200
1300
CHANNEL NUMBER

FIG. 5a

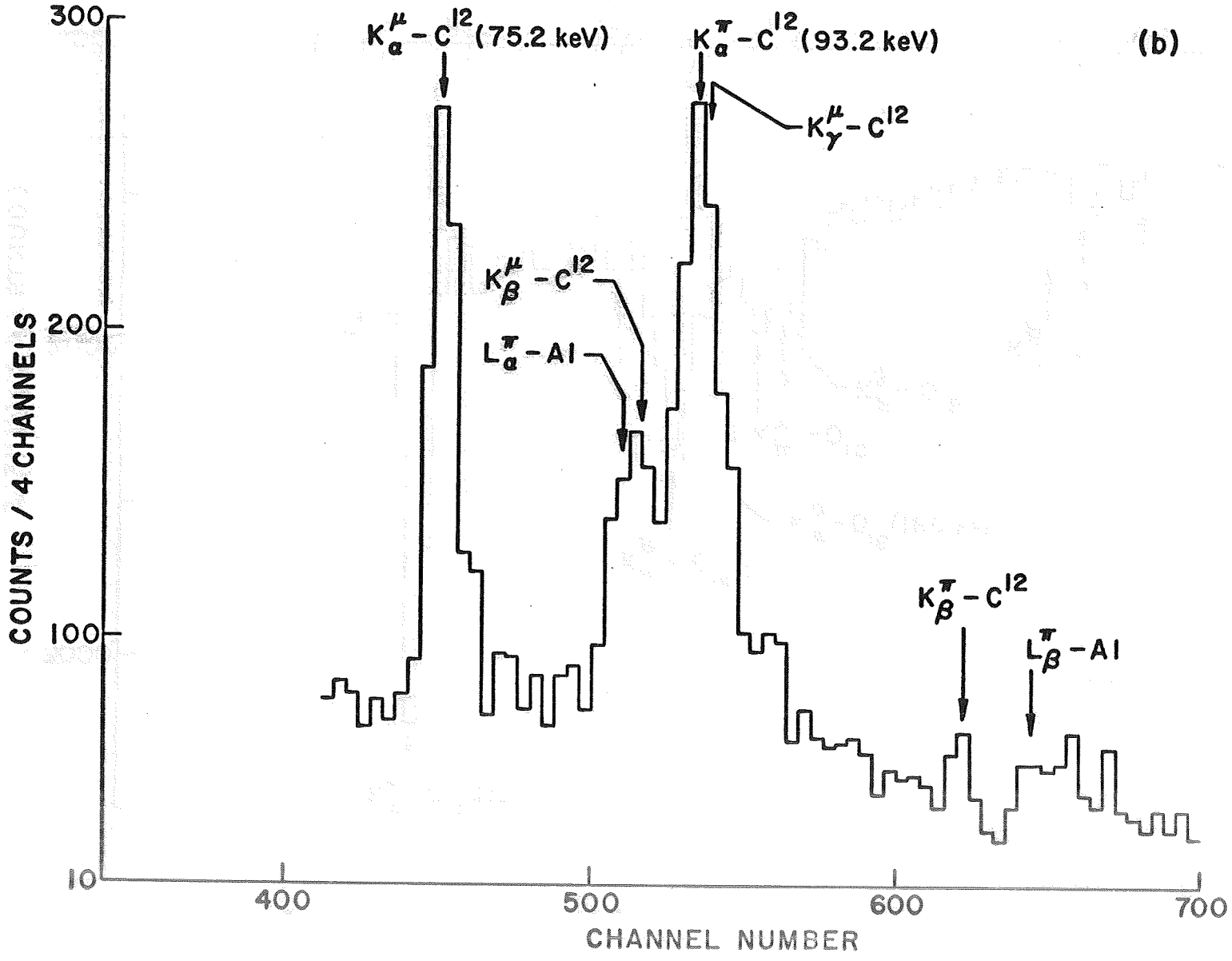
300
200
100
10
COUNTS / 4 CHANNELS
$K_\alpha^\mu - C^{12}$ (75.2 keV)
$K_\alpha^\pi - C^{12}$ (93.2 keV)
(b)
$K_\gamma^\mu - C^{12}$
$K_\beta^\mu - C^{12}$
$L_\alpha^\pi - Al$
$K_\beta^\pi - C^{12}$
$L_\beta^\pi - Al$
400
500
600
700
CHANNEL NUMBER

FIG. 5b

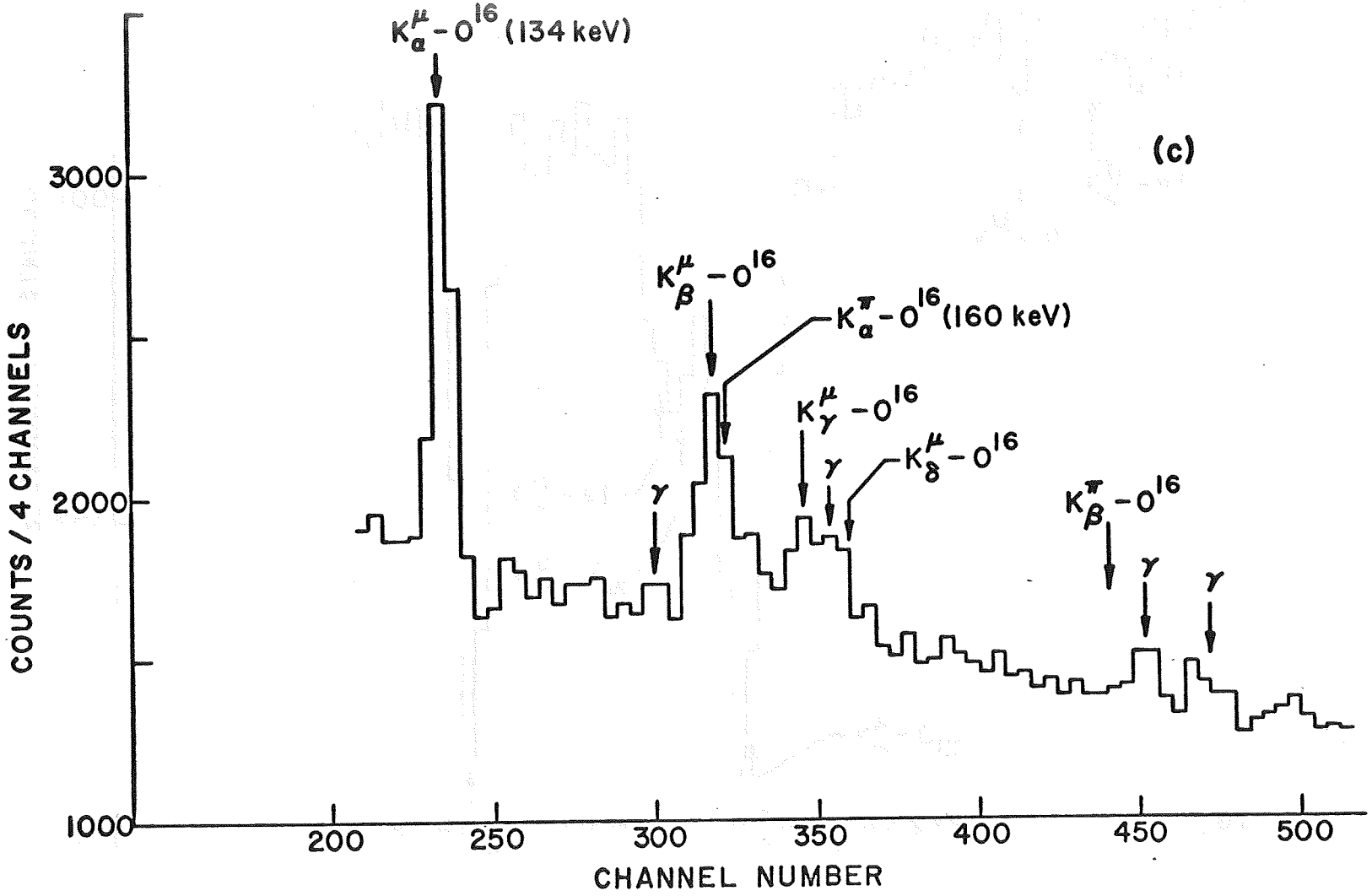
$K_\alpha^\mu - O^{16}$ (134 keV)
(c)
$K_\beta^\mu - O^{16}$
$K_\alpha^\pi - O^{16}$ (160 keV)
$K_\gamma^\mu - O^{16}$
$K_\delta^\mu - O^{16}$
$K_\beta^\pi - O^{16}$
γ
γ
γ
γ
3000
2000
1000
COUNTS / 4 CHANNELS
200
250
300
350
400
450
500
CHANNEL NUMBER

FIG. 5c

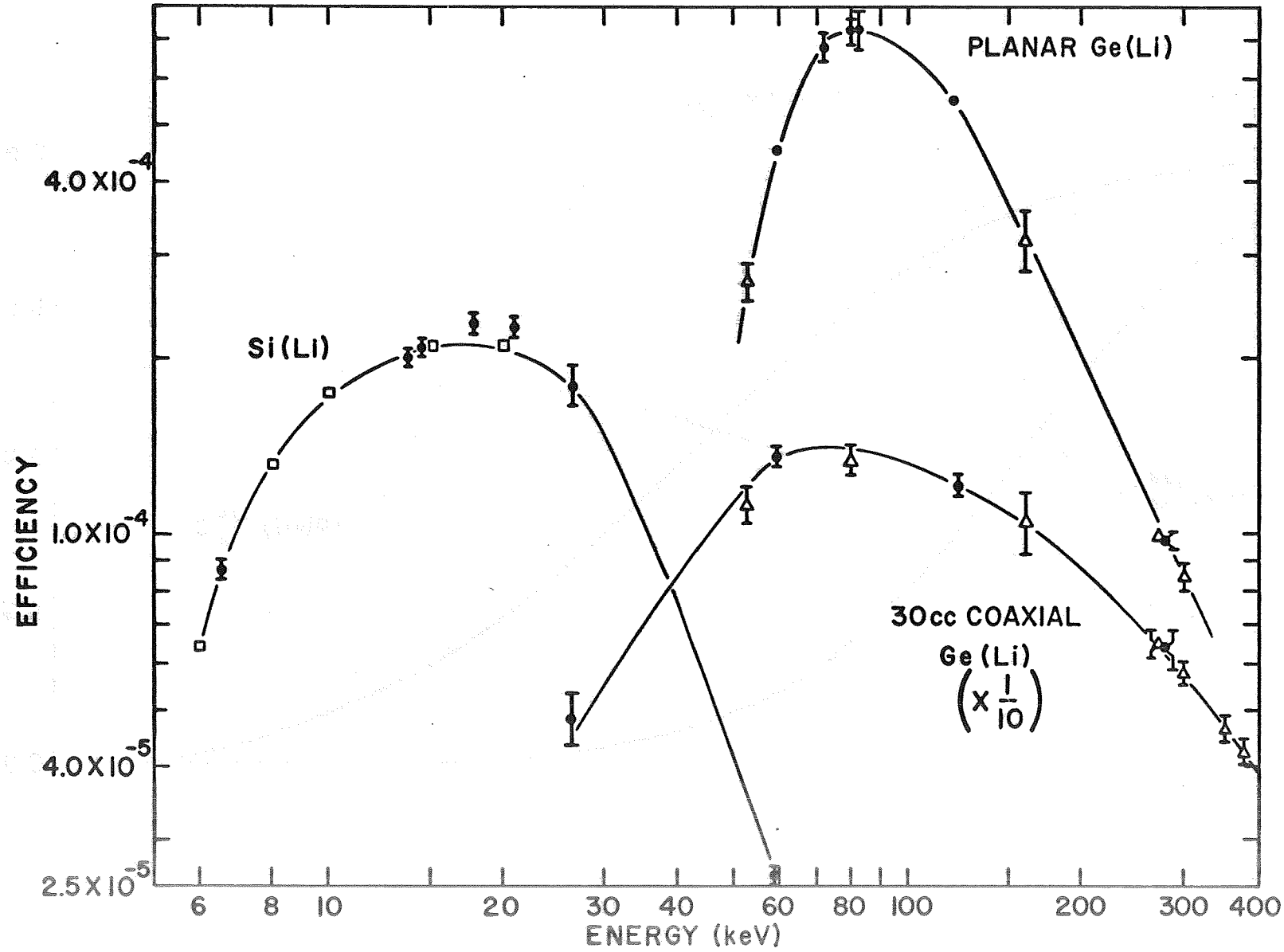
PLANAR Ge(LI)
Si(LI)
30cc COAXIAL
Ge (Li)
(X 1/10)
EFFICIENCY
4.0X10-4
1.0X10-4
4.0X10-5
2.5X10-5
6
8
10
20
30
40
60
80
100
200
300
400
ENERGY (keV)

FIG. 6

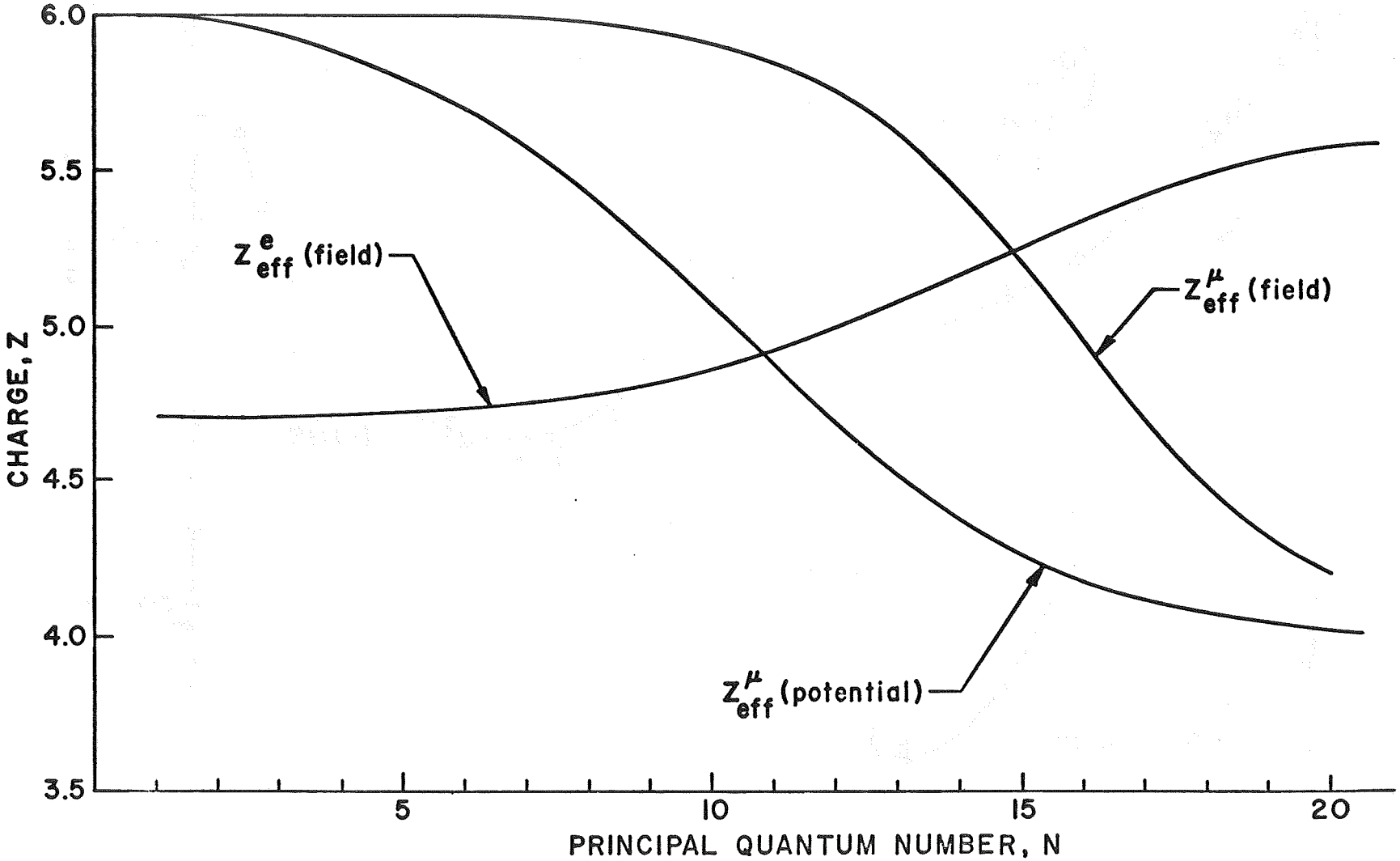
6.0
5.5
5.0
4.5
4.0
3.5
CHARGE, Z
5
10
15
20
PRINCIPAL QUANTUM NUMBER, N
Z^{e}_{eff} (field)
Z^{μ}_{eff} (field)
Z^{μ}_{eff} (potential)

FIG. 7

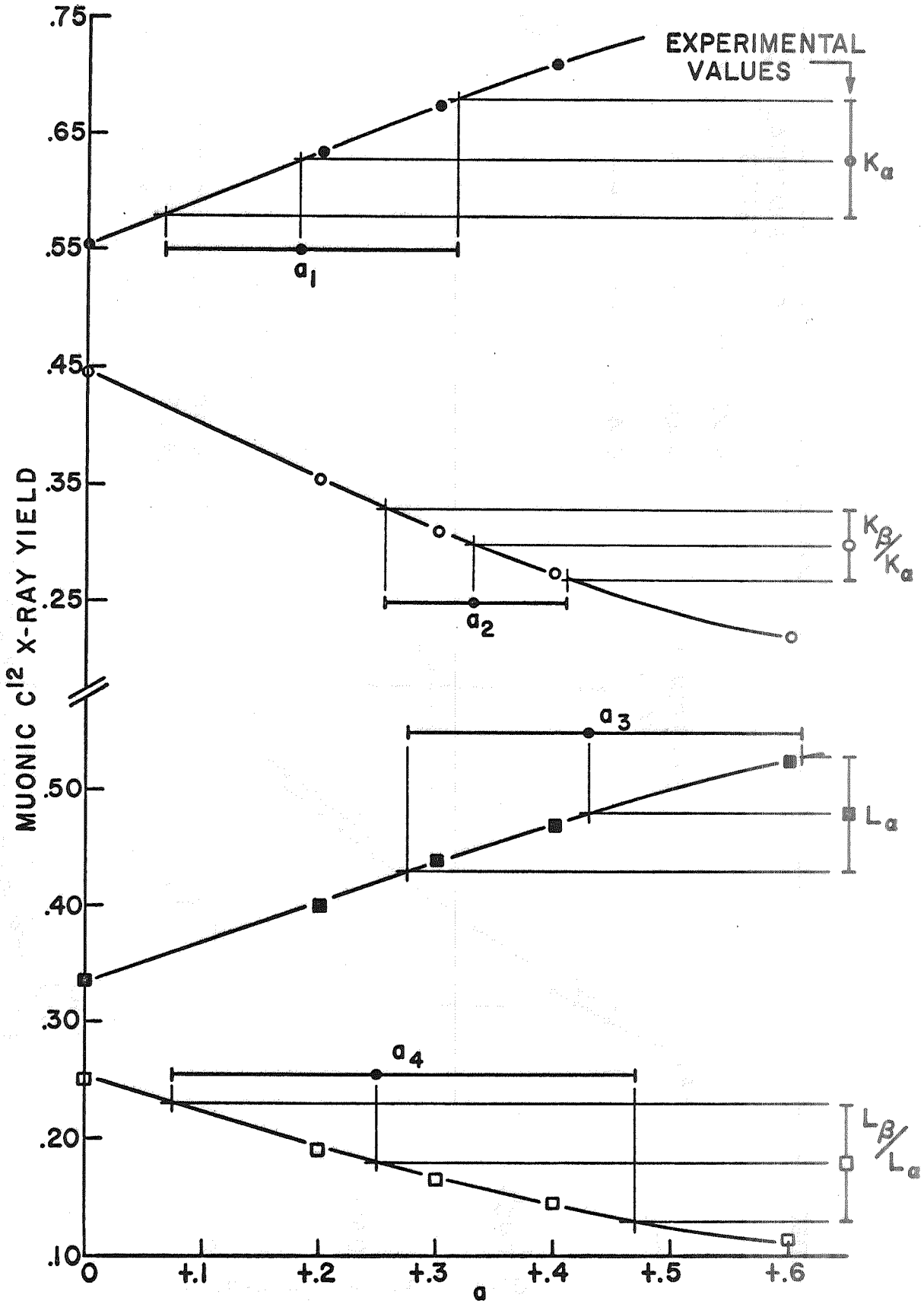
.75
.65
.55
.45
.35
.25
.50
.40
.30
.20
.10
0
+.1
+.2
+.3
+.4
+.5
+.6
a
MUONIC C12 X-RAY YIELD
EXPERIMENTAL VALUES
Kα
a1
Kβ/Kα
a2
a3
Lα
a4
Lβ/Lα

FIG. 8

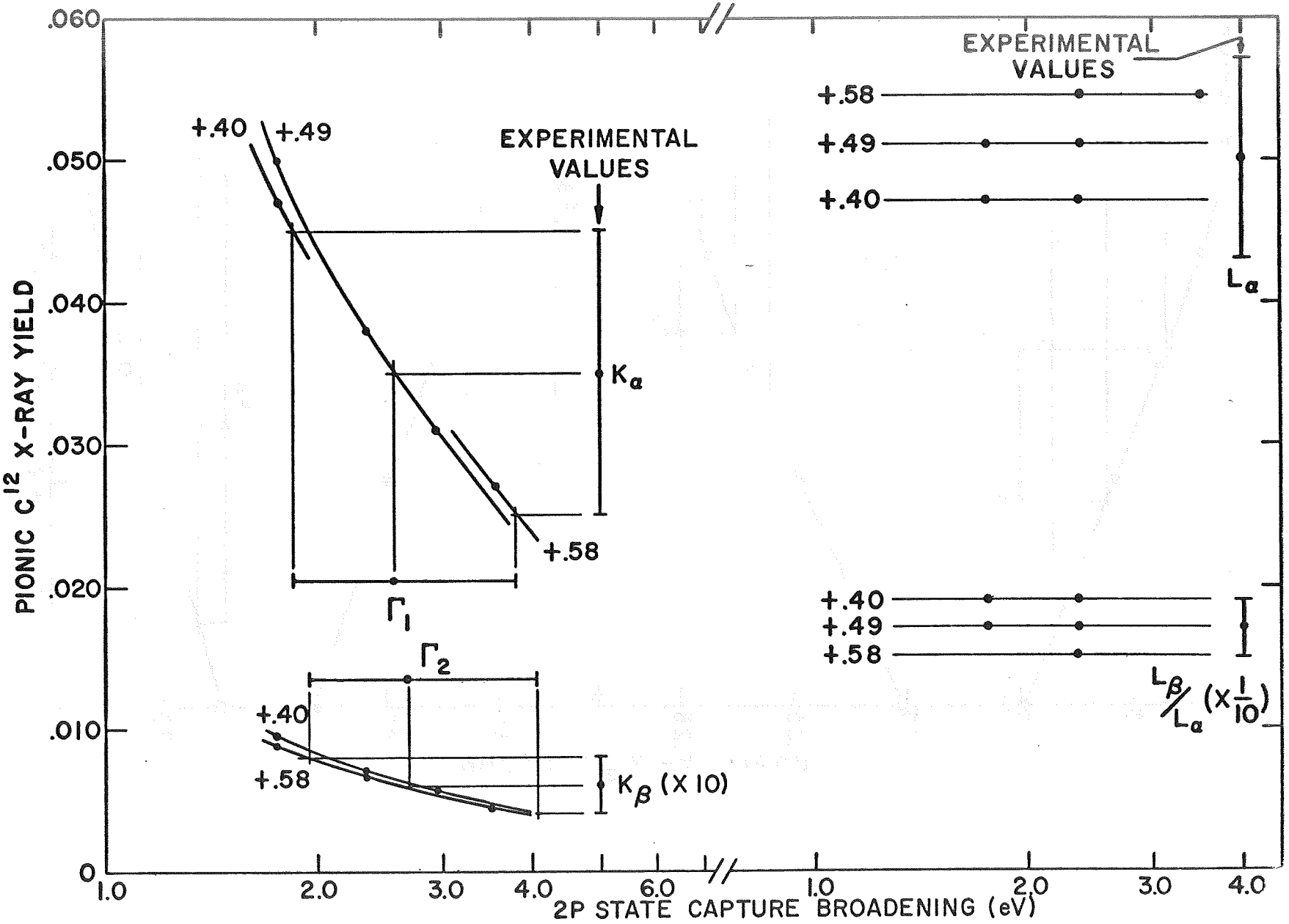
.060
.050
.040
.030
.020
.010
0
PIONIC C12 X-RAY YIELD
+.40
+.49
+.58
EXPERIMENTAL VALUES
Kα
Γ1
Γ2
Kβ (X 10)
EXPERIMENTAL VALUES
+.58
+.49
+.40
Lα
+.40
+.49
+.58
Lβ/Lα (X 1/10)
1.0
2.0
3.0
4.0
6.0
1.0
2.0
3.0
4.0
2P STATE CAPTURE BROADENING (eV)

FIG. 9

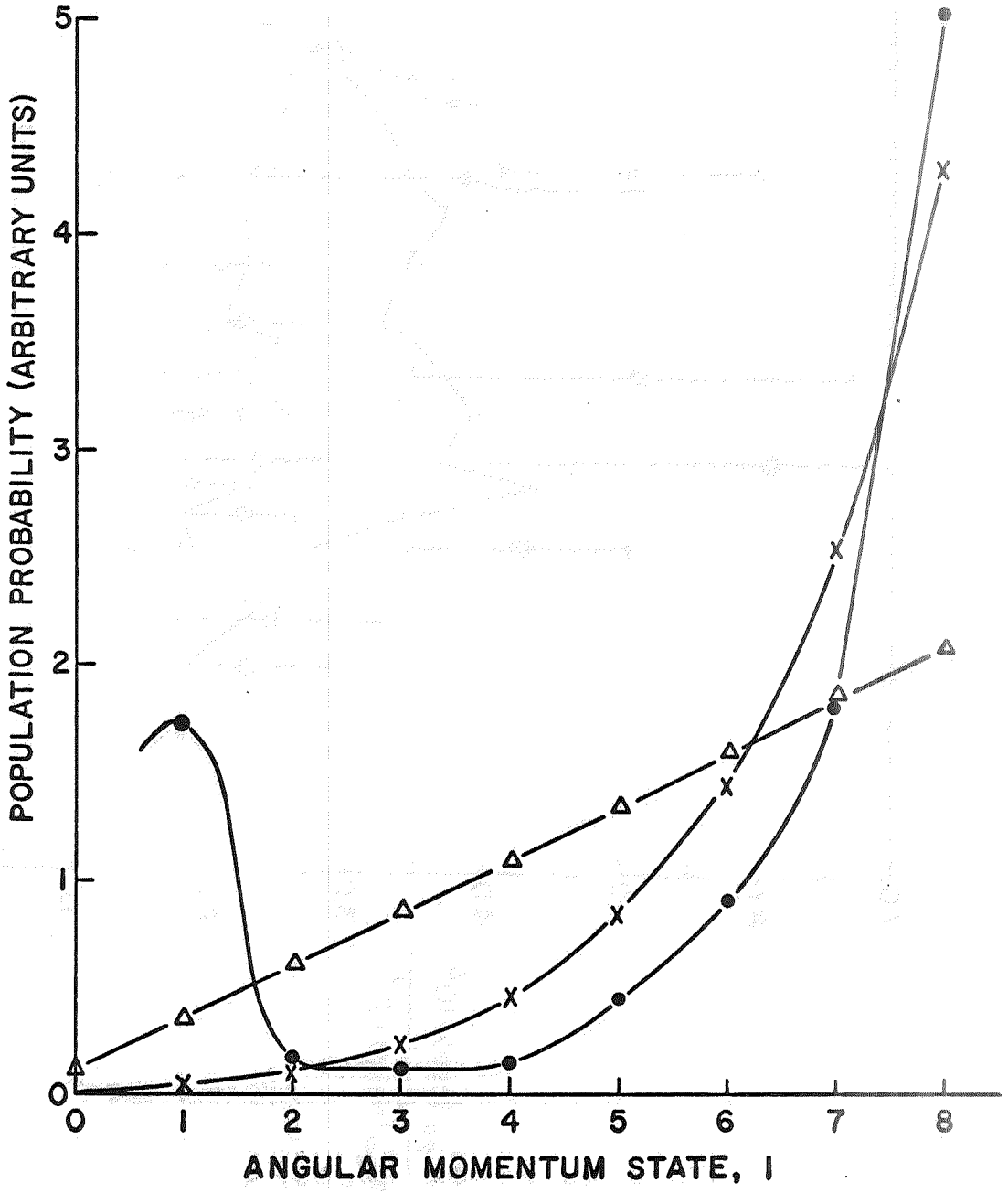
POPULATION PROBABILITY (ARBITRARY UNITS)
0
1
2
3
4
5
0
1
2
3
4
5
6
7
8
ANGULAR MOMENTUM STATE, l

FIG. 10

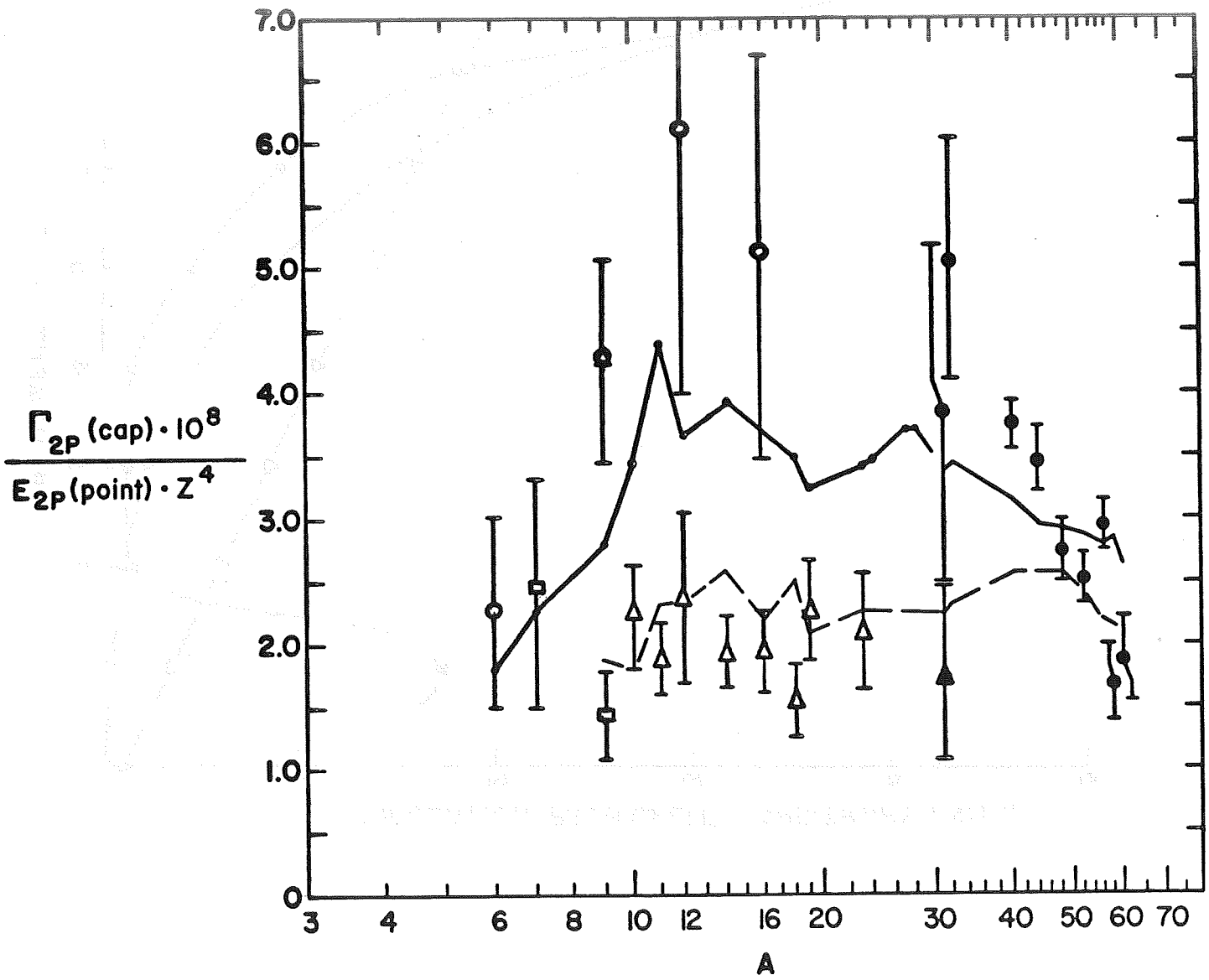
$\frac{\Gamma_{2P}(cap)\cdot 10^8}{E_{2P}(point)\cdot Z^4}$
7.0
6.0
5.0
4.0
3.0
2.0
1.0
0
3
4
6
8
10
12
16
20
30
40
50
60
70
A

FIG. 11